Modeling Hydrogen Metal Interactions

SAND2017-8922C

Xiaowang Zhou, R. B. Sills, M. E. Foster, R. A. Karnesky
Sandia National Laboratories

World Chemistry Conference & Exhibition
September 4-6, 2017, Rome, Italy

Sandia National Laboratories is a multi-mission laboratory managed and operated by National Technology and Engineering Solutions of Sandia, LLC., a wholly owned subsidiary of Honeywell International, Inc., for the U.S. Department of Energy's National Nuclear Security Administration under contract DE-NA-0003525.

Outline

Hydrogen-metal interaction impacts a variety of material problems including hydrogen storage, hydrogen embrittlement, tritium science, etc. Molecular dynamics is effective in studying these problems. Here discuss three topics:

- Molecular dynamics studies of grain boundary and irradiation effects on hydrogen diffusion in nickel
- Development of Fe-Ni-Cr interatomic potential
- Quantification and reduction of statistical uncertainties in molecular dynamics models

Grain Boundary and Irradiation effects on Hydrogen Diffusion in Nickel

- The TMIST-2 irradiation experiment at the Advanced Test Reactor at Idaho National Laboratory measured a tritium permeation enhancement in 316 stainless steel by a factor of ~2 to 5 relative to ex-reactor results
- Grain boundaries and irradiation-induced defects may be both responsible
- Statistics of diffusion cannot be captured by DFT calculations. Molecular dynamics (MD) simulations are required to understand this
- The literature stainless steel potential we found at the time was developed by Bonny et al, but their later version (MSMSE, 21, 85004, 2013) incorrectly predicts phase separation

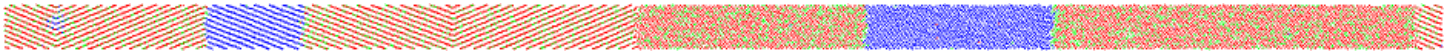

- We therefore use Ni as an exemplar to perform extensive MD simulations on hydrogen diffusion in Ni to elucidate the tritium permeation enhancement in 316 stainless steels

Sandia National Laboratories

Pacific Northwest NATIONAL LABORATORY

Molecular Dynamics Method

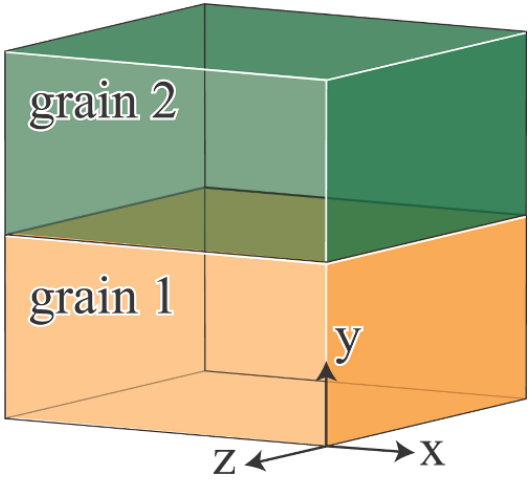

- Grain boundaries parallel to xz plane are simulated with bi-crystals under periodic boundary conditions
- Single crystal and Σ3{111}, Σ5{100), Σ11{311} grain boundaries are studied
- Systems with and without point defects are both considered. Three different point defects (interstitials, vacancies, and Frenkel pairs) are independently simulated. Defect concentration is fixed at contain C_{def} = 0.5%
- Systems contain a hydrogen concentration of C_H = 2%
- Ni-H potential from Angelo et al, MSMSE, 3, 289, 1995
- MD simulations are performed at 13 temperatures 300 K, 325 K, …, 575 K, 600 K for a period of t_{MD} = 440 ns (after 1 ns pre-equilibration)

Diffusion Analysis

- The coordinates $\alpha_i(t)$ of N hydrogen atoms (i = 1, 2, …, N), are recorded on a time interval of Δt, i.e., at times of $t = j\Delta t$, j = 1, 2, …, m ($m = t_{MD}/\Delta t$), where Δt can be any multiple of the time step size dt used in the MD simulations.
- m+1-k measurements can be made for the displacement of a hydrogen atom i over a $k\Delta t$ period: $\Delta\alpha_{i,j}(k\Delta t) = \alpha_i(j\Delta t - \Delta t + k\Delta t) - \alpha_i(j\Delta t - \Delta t)$ where j = 1, 2, …, m+1-k.
- This allows us to calculate mean square displacement (MSD):

$$\left\langle \left[\Delta\alpha(k\Delta t)\right]^2 \right\rangle = \frac{\sum_{i=1}^{N}\sum_{j=1}^{m+1-k}\left[\Delta\alpha_{i,j}(k\Delta t)\right]^2}{N(m+1-k)}$$

- MSD can be fitted to diffusivities D:

$$\left\langle \left[\Delta\alpha(k\Delta t)\right]^2 \right\rangle = 2D_\alpha t$$
$$\left\langle \left[\Delta x(k\Delta t)\right]^2 \right\rangle + \left\langle \left[\Delta z(k\Delta t)\right]^2 \right\rangle = 4D_{xz} t$$
$$\left\langle \left[\Delta x(k\Delta t)\right]^2 \right\rangle + \left\langle \left[\Delta y(k\Delta t)\right]^2 \right\rangle + \left\langle \left[\Delta z(k\Delta t)\right]^2 \right\rangle = 6D_{xyz} t$$

MSD convergence figure

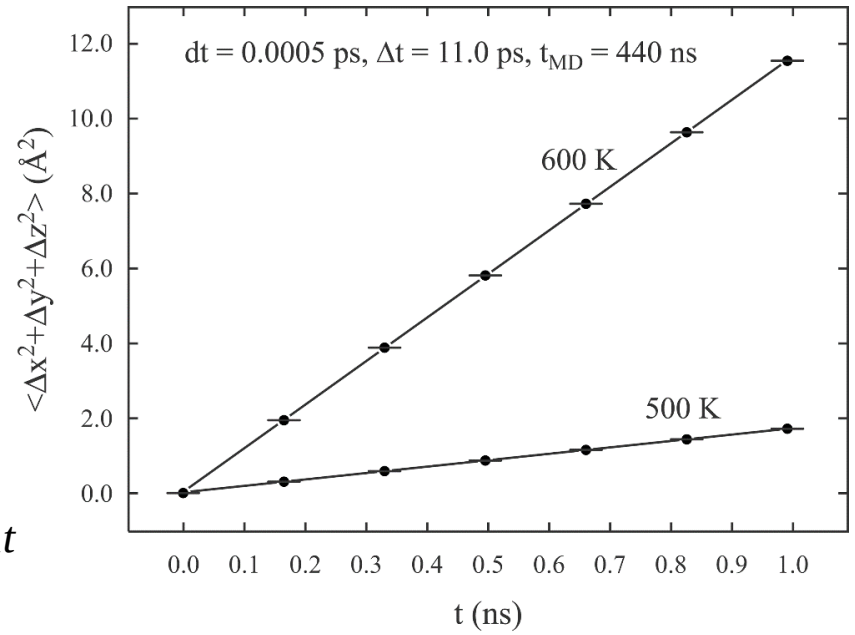

Sandia National Laboratories

Pacific Northwest NATIONAL LABORATORY

Defect Effects on H Diffusion in Ni Single Crystals

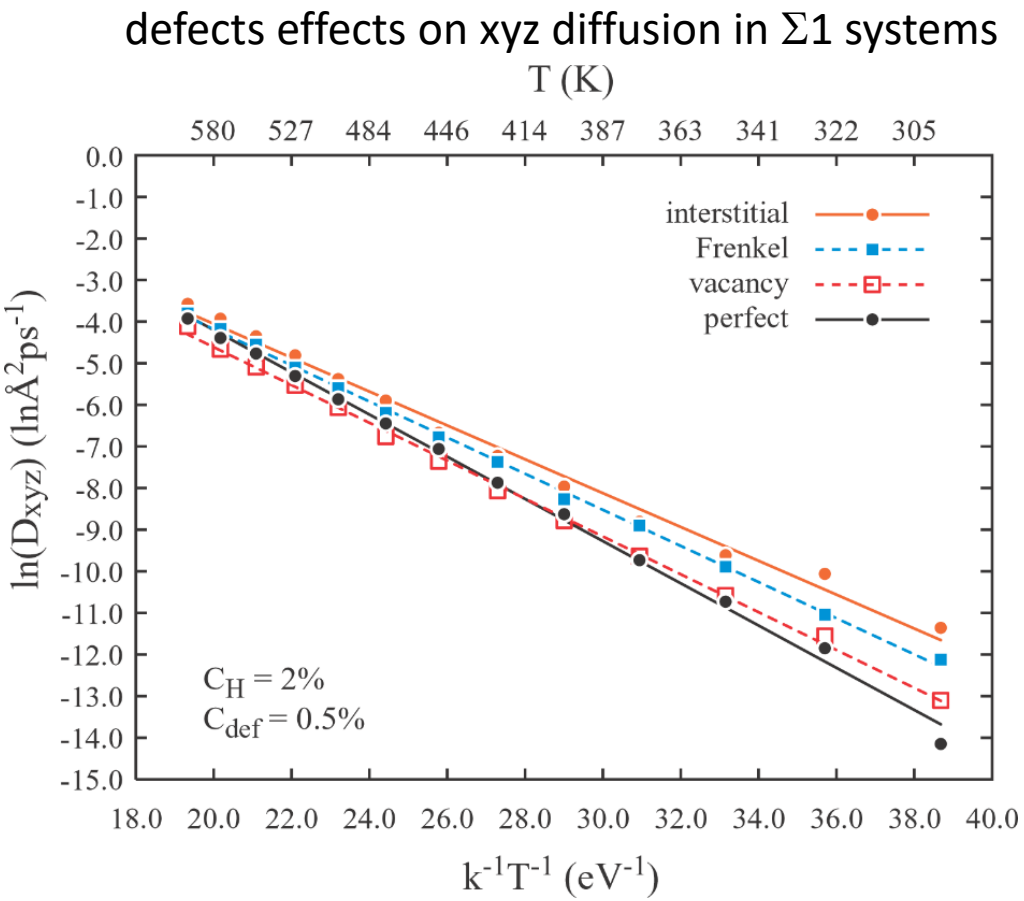

- Diffusivities are close with and without vacancies
- At the simulated interstitial concentration of 0.5%, interstitial increases diffusivities by 16.3 times at 300 K and 1.4 times at 600 K as compared with perfect crystals
- Activation energy of diffusion for perfect crystals is predicted to be 0.51 eV, as compared to the experimental value of 0.40 eV*

*L. Katz, M. Guinan, and R. J. Borg, Phys. Rev. B, 4, 330 (1971)

t = 440 ns

Sandia National Laboratories

Pacific Northwest NATIONAL LABORATORY

Defect Effects on H Diffusion in Ni with the Σ3{111} GB

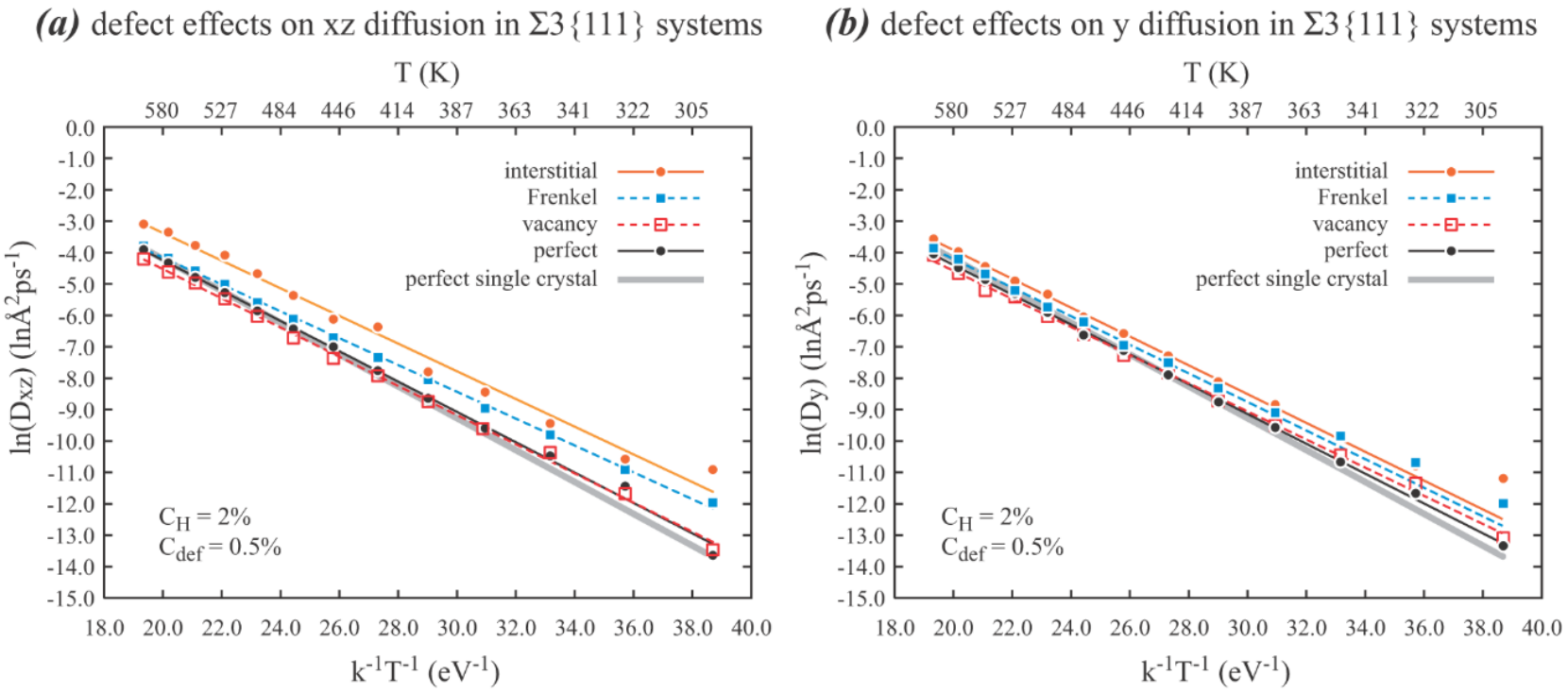

- The coherent twin boundary almost has no effects on diffusivities with different defects except in the interstitial case
- Interstitial increases on-plane diffusivities by 15.3 times at 300 K and 2.3 times at 600 K as compared with perfect crystals
- Out-plane diffusivities are close to single crystals, indicating insignificant grain boundary trapping

t = 440 ns

Sandia National Laboratories

Pacific Northwest NATIONAL LABORATORY

Visualization of Σ3{111} Grain Boundary

$C_H = 2\%$
$C_{def} = 0.5\%$

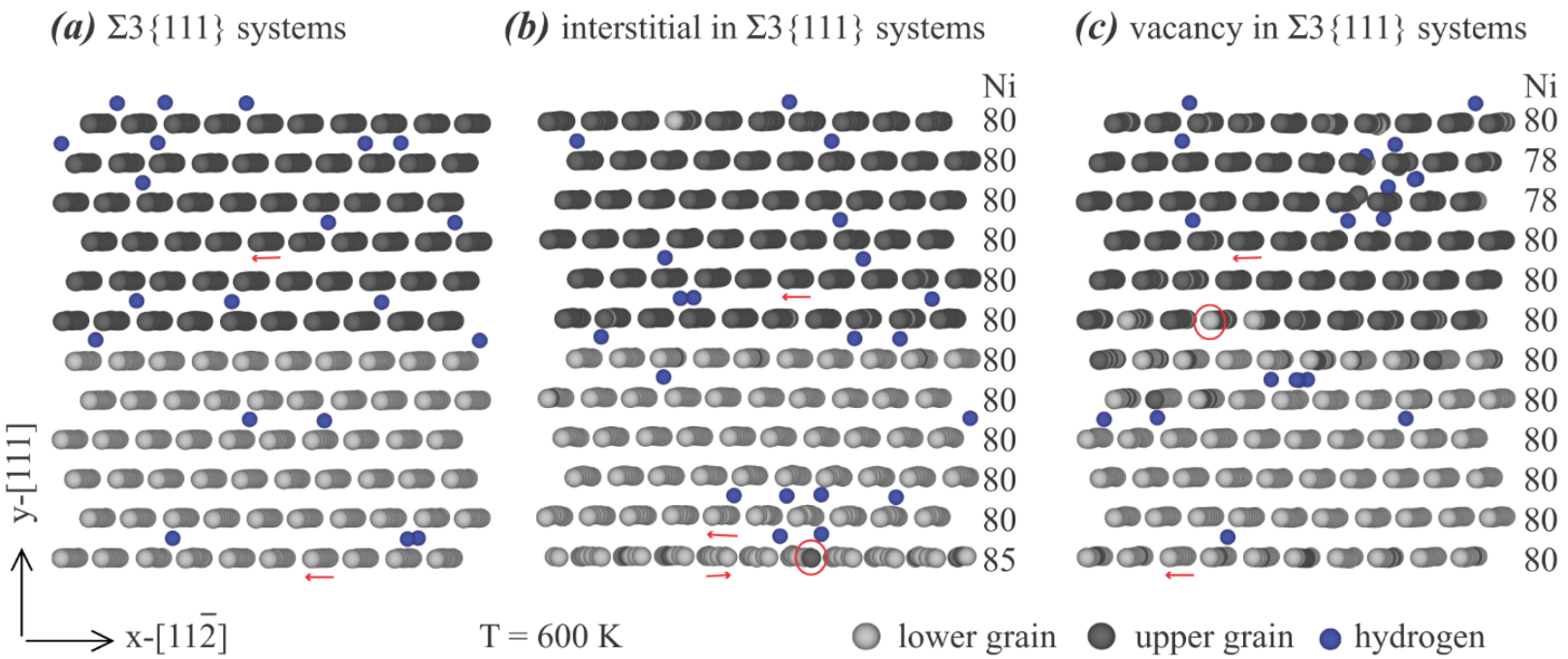

- Hydrogen does not segregate, but Ni interstitials and vacancies segregate at grain boundary
- Ni diffusion only occurs at the presence of interstitials and vacancies
- Interstitials cause reconstructions of atomic rows

Sandia National Laboratories

Pacific Northwest NATIONAL LABORATORY

Observation of Two Σ3{111} Grain Boundary Reconstructions due to Interstitials

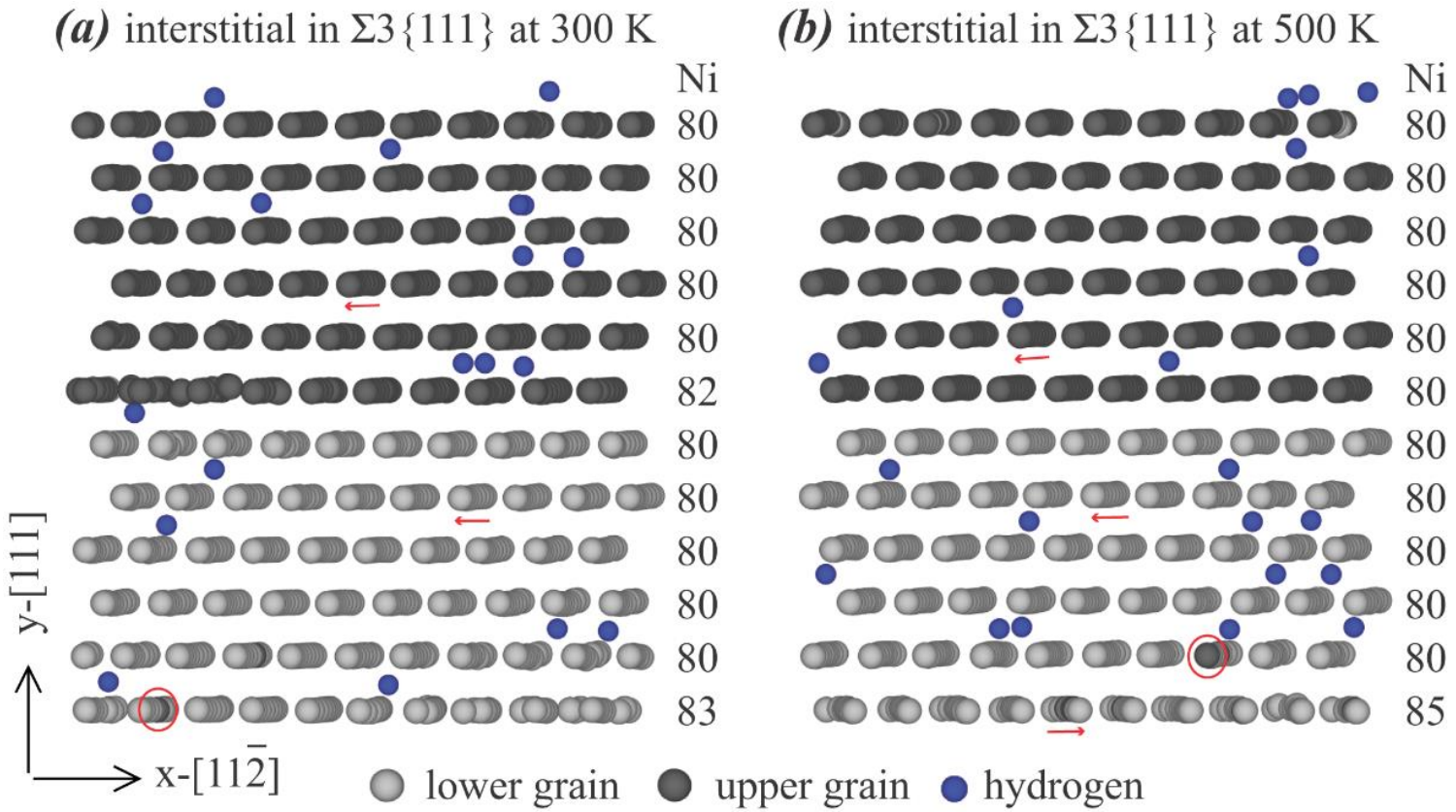

- The 300 K reconstruction is similar to the one shown above, but the atomic rows in the 500 K reconstruction are different

C_H = 2%,
C_{def} = 0.5%

Sandia National Laboratories

Pacific Northwest NATIONAL LABORATORY

Statistical Effects of Initial Σ3{111} GB Reconstructions

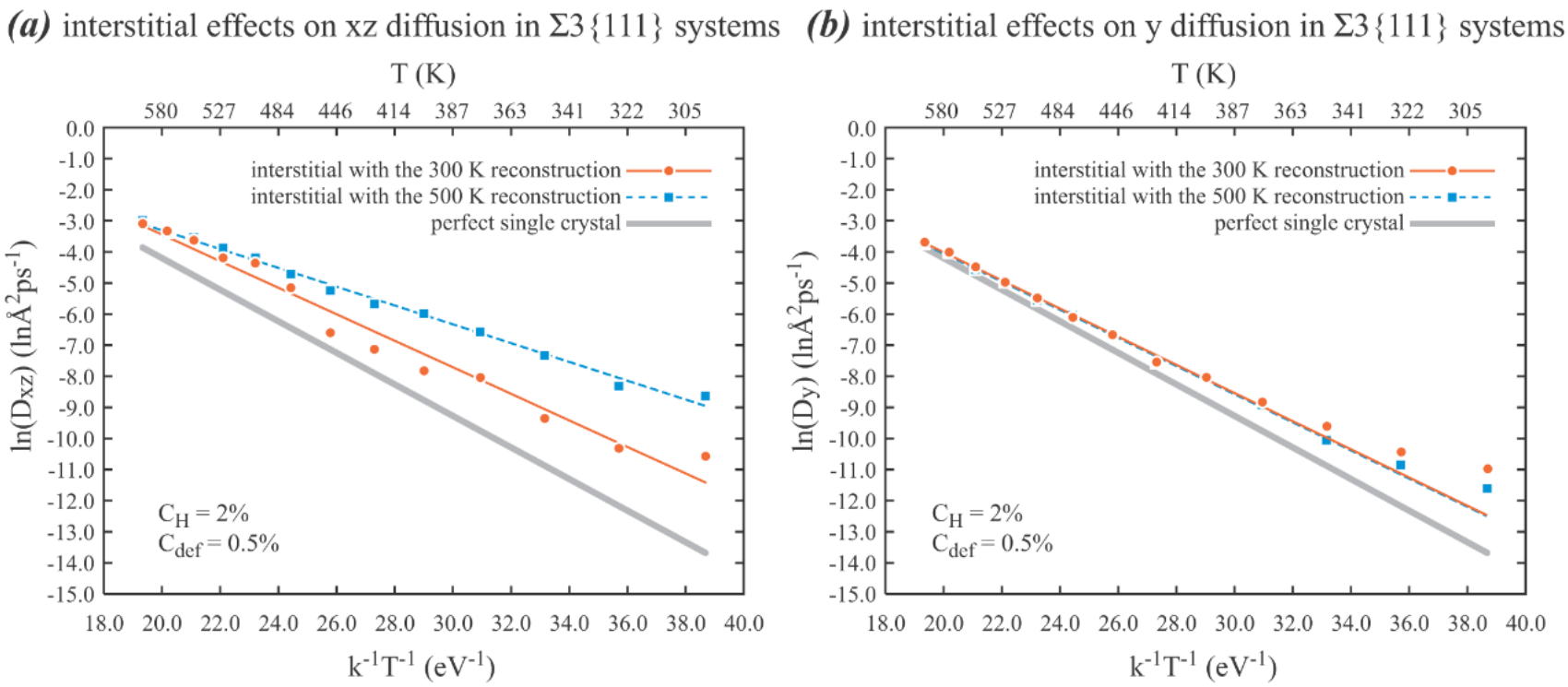

- Depending on reconstruction, the combination of interstitials and the Σ3{111} grain boundary may significantly increase the on-plane diffusivities
- Interstitial increases on-plane diffusivities by 146.7 times at 300 K and 2.4 times at 600 K as compared with the boundary alone case
- Out-plane diffusivity is not significantly affected

t = 440 ns

Sandia National Laboratories

Pacific Northwest NATIONAL LABORATORY

Defect Effects on H Diffusion in Ni with Σ5{100} GB

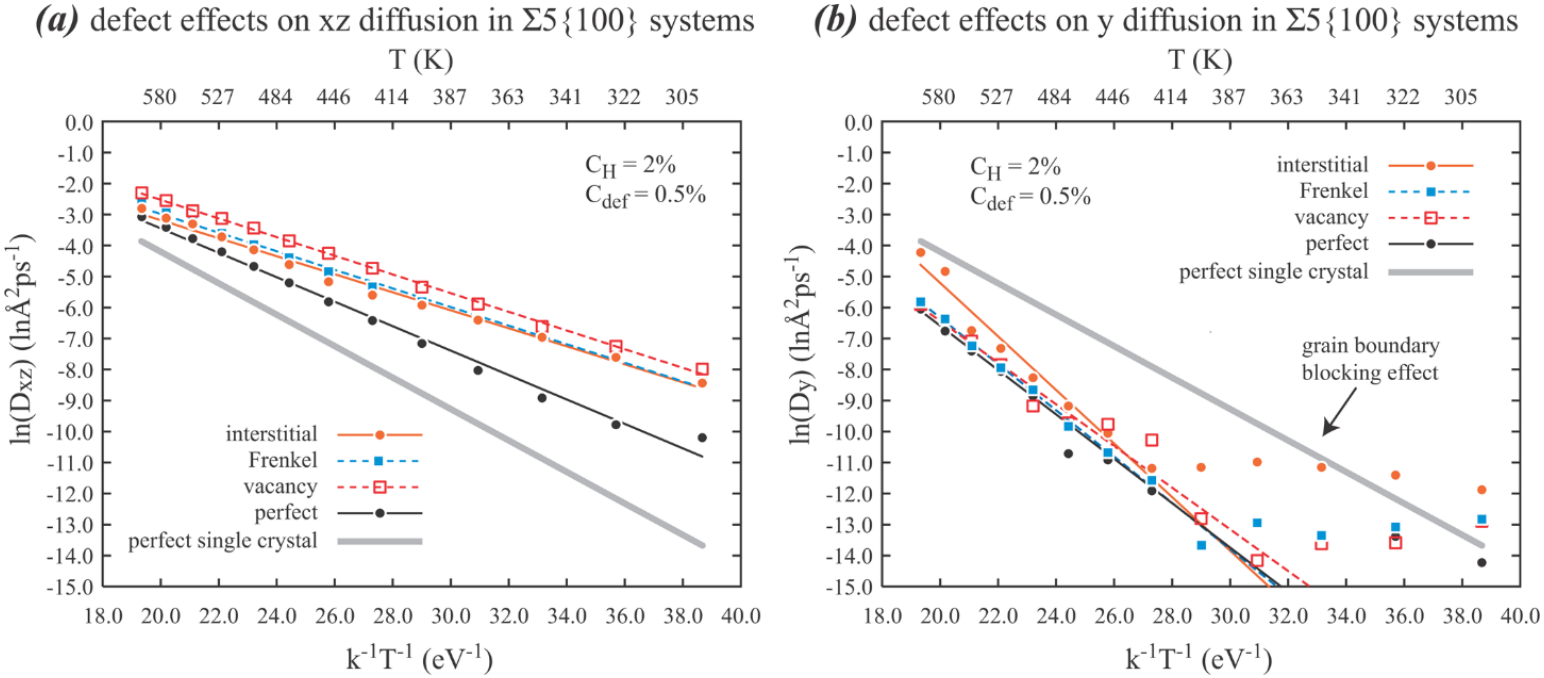

- The Σ5{100} GB itself significantly increases the on-plane diffusion (relative to single crystal)
- All defects increase the on-plane diffusivities, especially vacancies (in single crystals, interstitials have the biggest effects and vacancies have negligible effects)
- Vacancy increases on-plane diffusivities by 9.2 times at 300 K and 2.2 times at 600 K as compared with the boundary alone case
- The out-plane diffusivities are significantly reduced as compared to bulk diffusion, indicating boundary trapping that is confirmed by the two segments

t = 440 ns

Sandia National Laboratories

Pacific Northwest NATIONAL LABORATORY

Visualization of Σ5{100} Grain Boundary

$C_H = 2\%$
$C_{def} = 0.5\%$

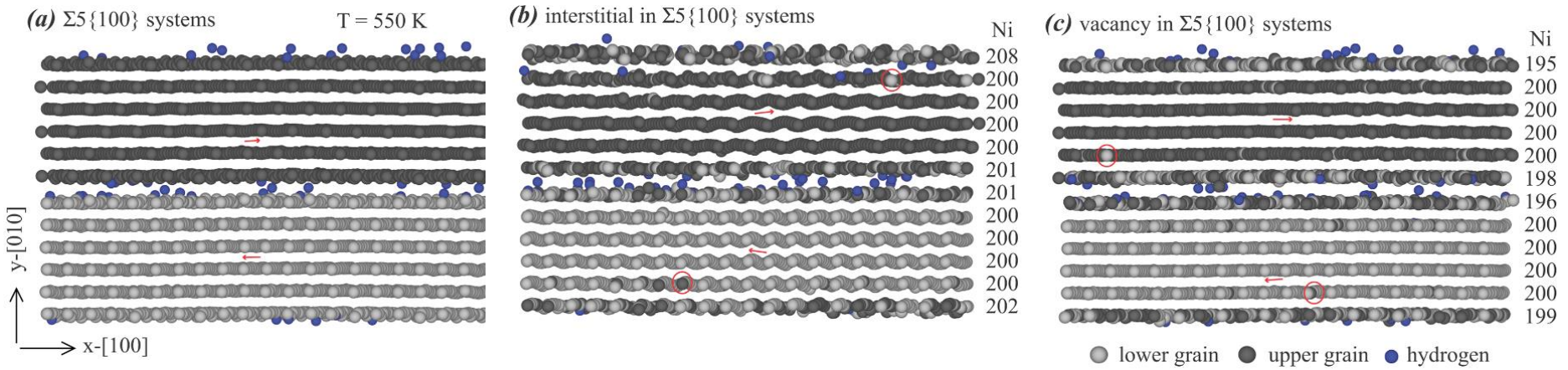

- Hydrogen atoms strongly segregates at the GB
- Ni interstitials and vacancies strongly segregate at the GB
- No change in the orientation of atomic rows
- Ni diffusion only occurs when ether interstitials or vacancies are present
- No statistical effects of initial configurations on diffusivities were found

Sandia National Laboratories

Pacific Northwest NATIONAL LABORATORY

Defect Effects on H Diffusion in Ni with Σ11{311} GB

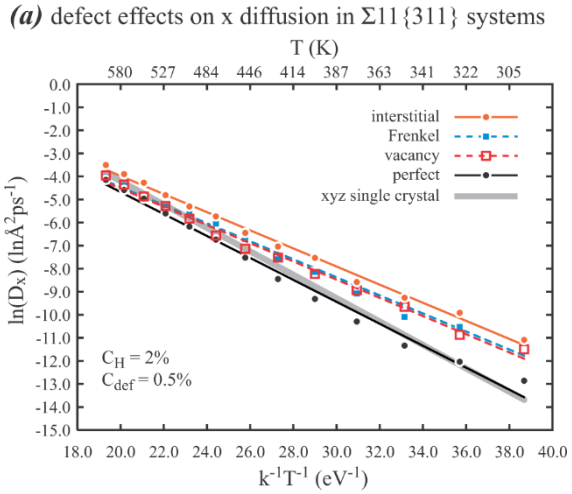

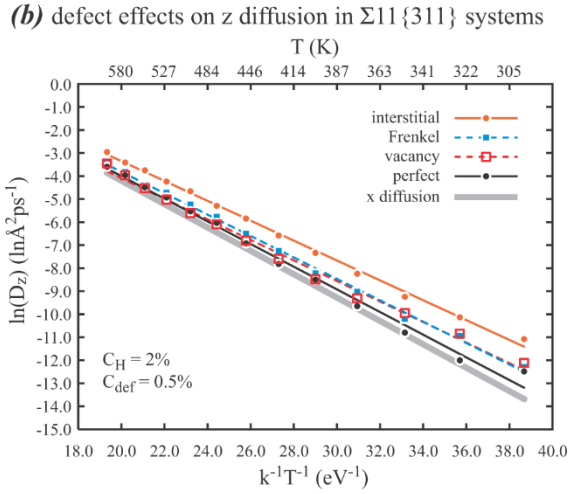

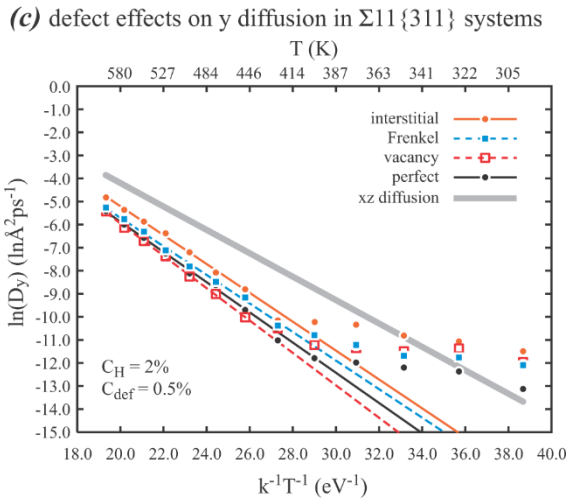

- Diffusivities in the two on-plane directions slightly differ
- Defects increase on-plane diffusivities especially at low temperatures
- Interstitials most significantly increase on-plane diffusivities
- In the x- direction, interstitials increase diffusivities by 5.9 times at 300 K and 1.9 times at 600 K as compared with the boundary alone case
- In the z- direction, interstitials increase diffusivities by 4.1 times at 300 K and 1.9 times at 600 K as compared with the boundary alone case
- The out-plane diffusivities are significantly reduced as compared to bulk diffusion, indicating boundary trapping that is confirmed by the two segments

t = 440 ns

Sandia National Laboratories

Pacific Northwest NATIONAL LABORATORY

Visualization of Σ11{311} Grain Boundary

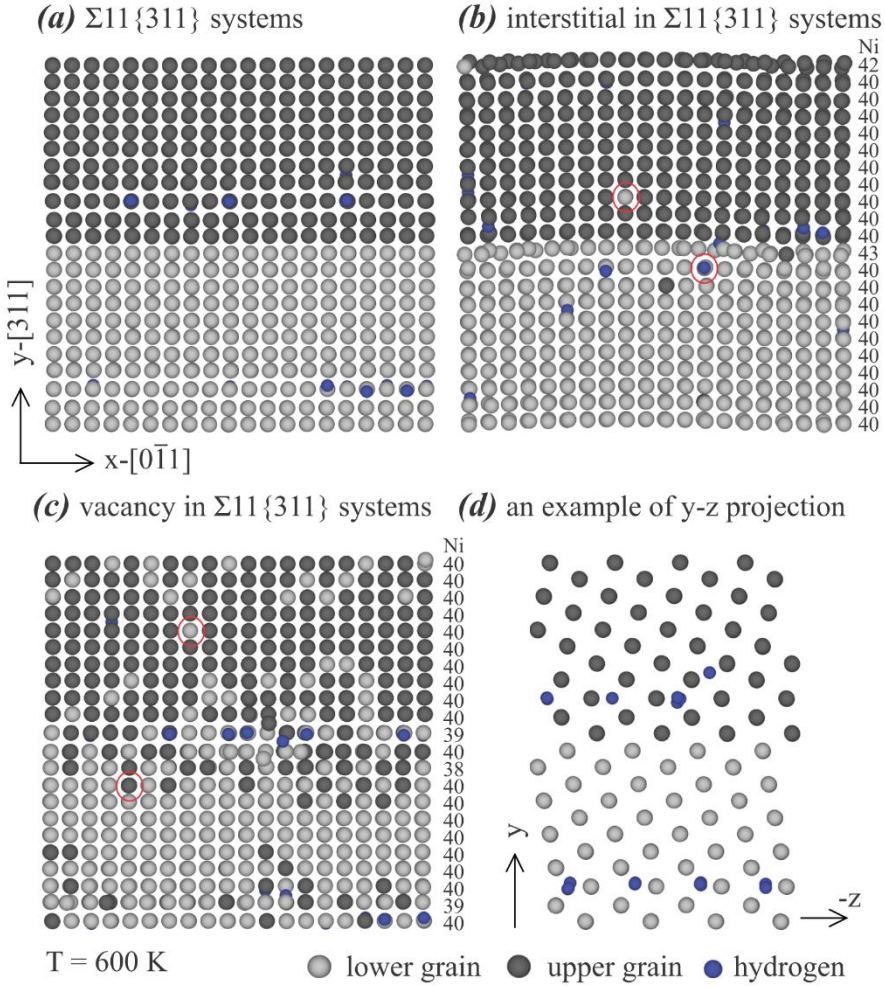

- Hydrogen atoms strongly segregates at the GB
- Ni interstitials and vacancies strongly segregate at the GB
- No change in the orientation of atomic rows
- Ni diffusion only occurs when ether interstitials or vacancies are present
- No statistical effects of initial configurations on diffusivities were found

$C_H = 2\%$, $C_{def} = 0.5\%$

Sandia National Laboratories

Pacific Northwest NATIONAL LABORATORY

Activation Energy and Pre-exponential Factors

Table I. Activation energies Q and pre-exponential factors D_0 for different cases. Note that subscript "xyz" indicates isotropic bulk diffusion, "y" indicates out-plane diffusion, "xz" indicate isotropic in-plane diffusion, "x" and "z" indicate that the anisotropic in-plane diffusion is further split into two directions.

	No defects	Vacancies	Interstitials		Frenkel pairs
	Single crystals				
Q_{xyz} (eV)	0.508	0.455	0.407		0.435
$D_{0,xyz}$ (Å^2/ps)	3.835×10^{2}	8.925×10^{1}	5.959×10^{1}		9.075×10^{1}
	Σ3{111}				
Q_{xz} (eV)	0.483	0.465	0.441	0.302	0.427
$D_{0,xz}$ (Å^2/ps)	2.283×10^{2}	1.190×10^{2}	2.336×10^{2}	1.553×10^{1}	8.116×10^{1}
Q_y (eV)	0.475	0.448	0.459	0.453	0.455
$D_{0,y}$ (Å^2/ps)	1.666×10^{2}	8.089×10^{1}	1.941×10^{2}	1.503×10^{2}	1.352×10^{2}
	Σ5{100}				
Q_{xz} (eV)	0.395	0.301	0.291		0.300
$D_{0,xz}$ (Å^2/ps)	8.623×10^{1}	3.376×10^{1}	1.413×10^{1}		2.073×10^{1}
Q_y (eV)	0.716	0.672	0.864		0.747
$D_{0,y}$ (Å^2/ps)	2.289×10^{3}	1.116×10^{3}	1.767×10^{5}		5.497×10^{3}
	Σ11{311}				
Q_x (eV)	0.476	0.395	0.393		0.391
$D_{0,x}$ (Å^2/ps)	1.271×10^{2}	2.907×10^{1}	4.808×10^{1}		2.888×10^{1}
Q_z (eV)	0.493	0.447	0.432		0.465
$D_{0,z}$ (Å^2/ps)	3.474×10^{2}	1.262×10^{2}	1.983×10^{2}		2.420×10^{2}
Q_y (eV)	0.655	0.703	0.627		0.620
$D_{0,y}$ (Å^2/ps)	1.388×10^{2}	3.342×10^{2}	1.528×10^{2}		8.077×10^{2}

$C_H = 2\%$

$C_{def} = 0.5\%$

Point defects + grain boundaries can reduce on-plane diffusion energy barrier, in agreement with experiments*

*A. Qudriss, J. Creus, J. Bouhattate, E. Conforto, C. Berziou, C. Savall, and X. , Acta Mater., 60, 6814 (2012).

Table II. Hydrogen-defect interaction energy (eV).

Point defects		Grain boundaries		
Vacancies	Interstitials	Σ3{111}	Σ5{100}	Σ11{311}
-0.18	-0.12	-0.03	-0.20	-0.24

By placing hydrogen at different locations, MD simulations at 100 K are used to calculate time-averaged interaction energies between hydrogen and various defects

Activation Energy of Individual Jumps

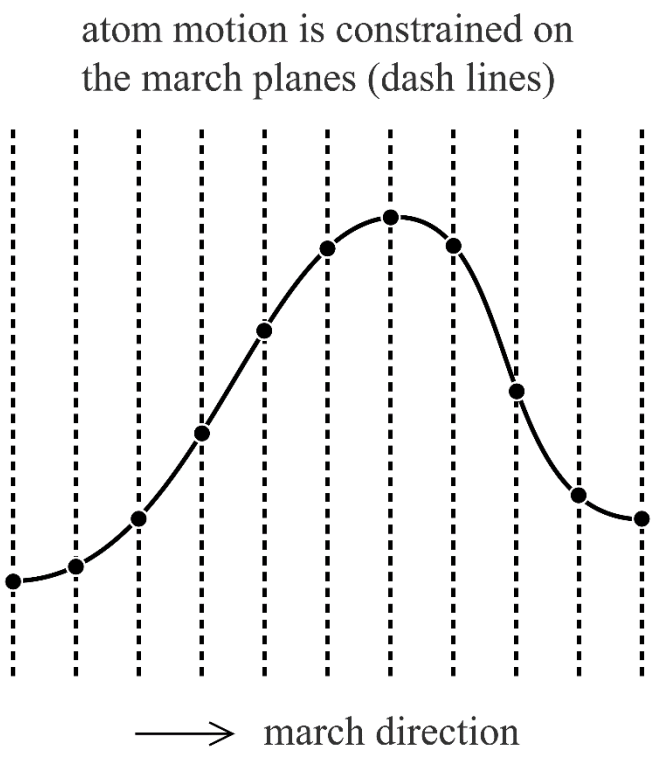

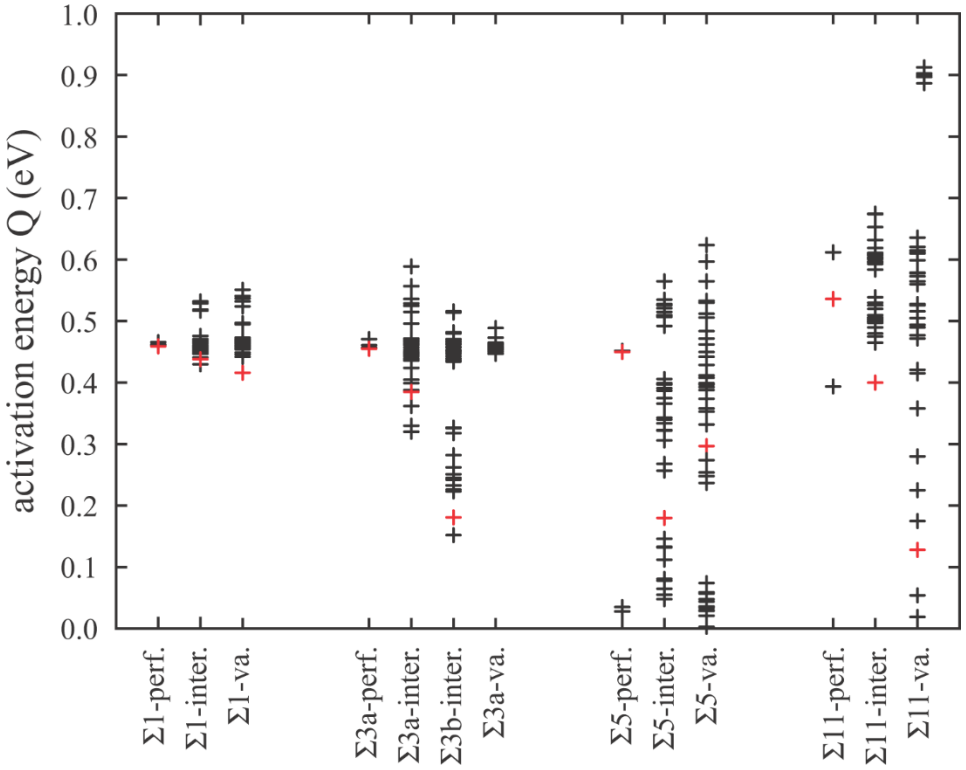

- By sequentially marching the hydrogen atoms in the three coordinate directions and relaxing the structure with the marching atom constrained on the marching plane, molecular statics can be used to calculate the energy barrier of atomic jumps
- This method can be easily automated to calculate a variety of atomic jumps

Visualization of Atomic Jumps in Single Crystal

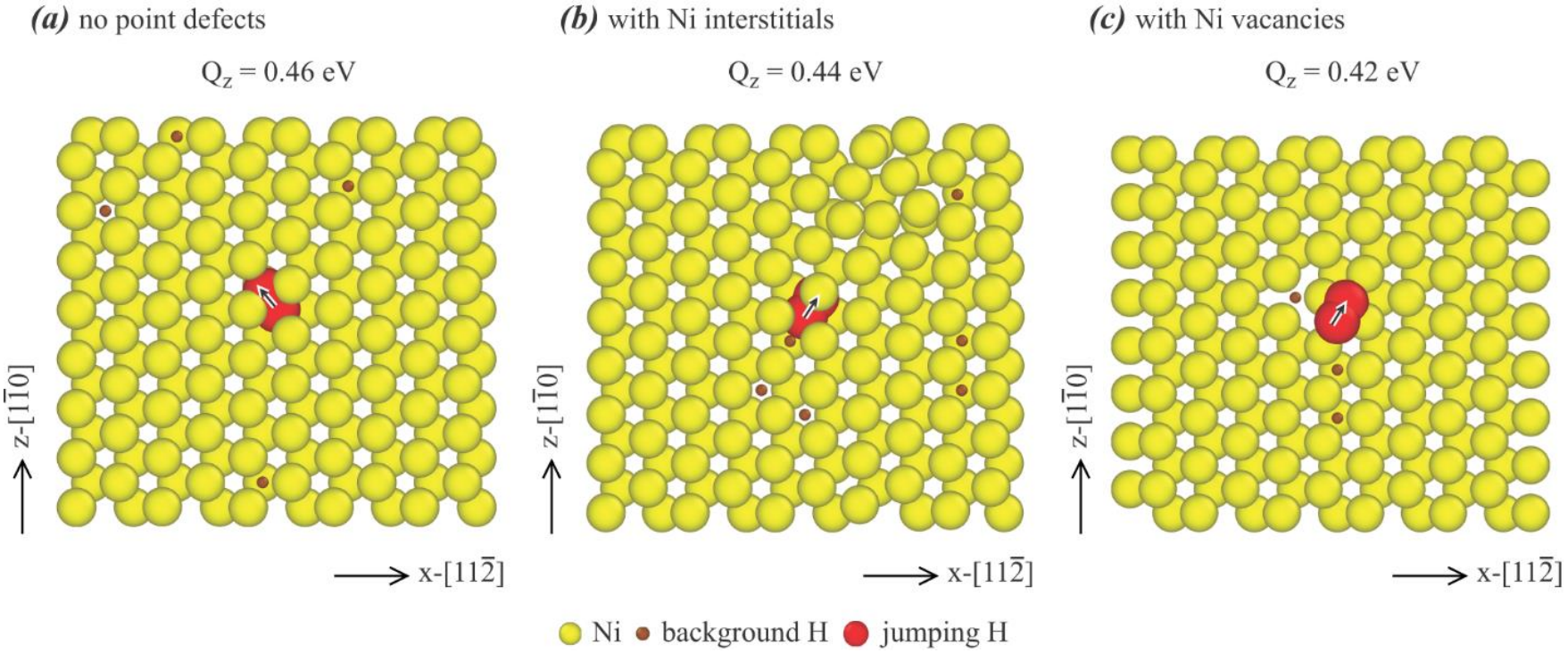

Presence of nickel interstitials or vacancies can reduce the energy barrier of some hydrogen jump paths, but not too much

Visualization of Atomic Jumps near the Σ3 GB

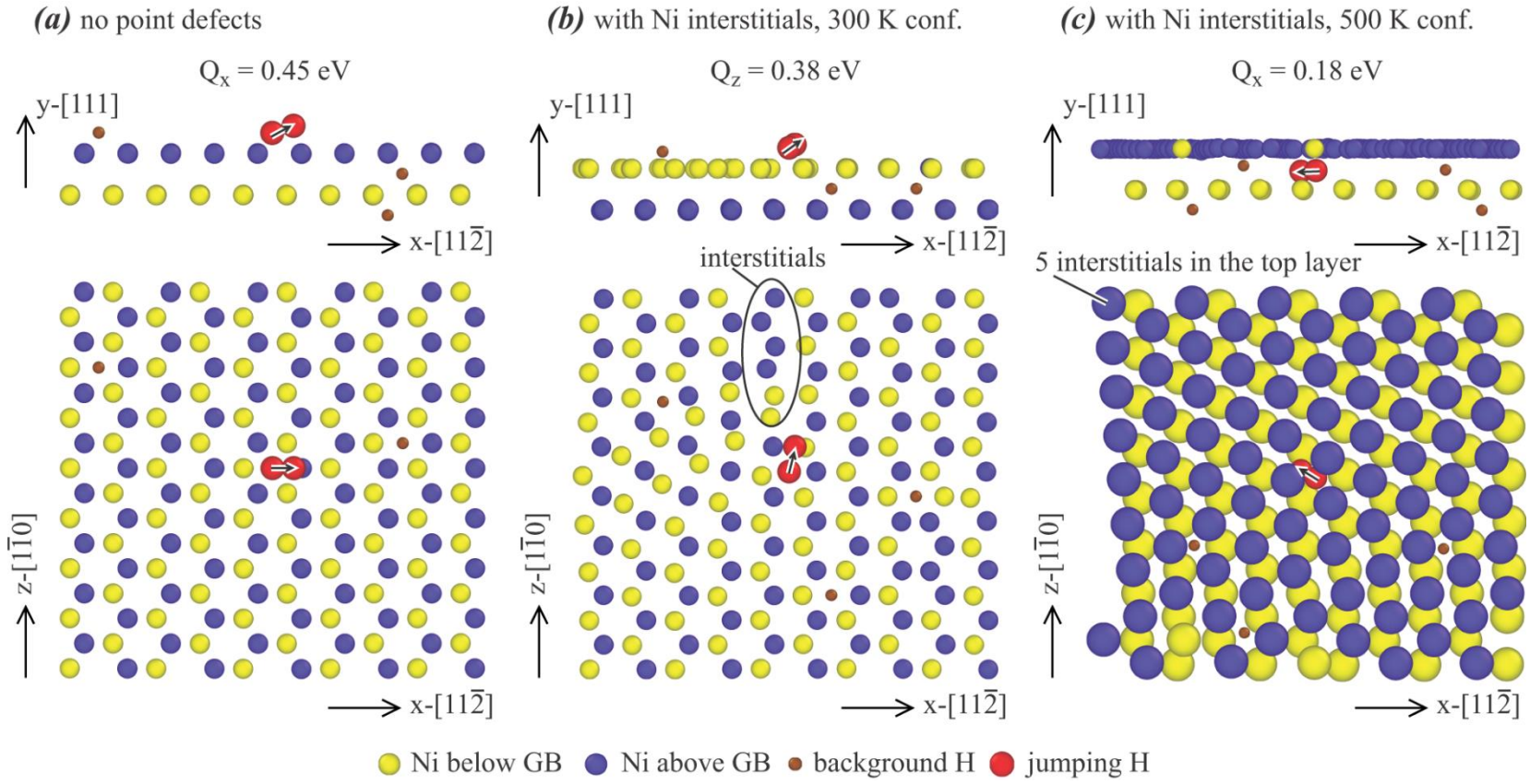

- Presence of nickel interstitials or vacancies can reduce the energy barrier of some hydrogen jump paths further from GB effects alone
- The 500 K initial configuration more effectively reduces the energy barrier because the 5 nickel interstitials are uniformly distributed

Visualization of Atomic Jumps near the Σ5 GB

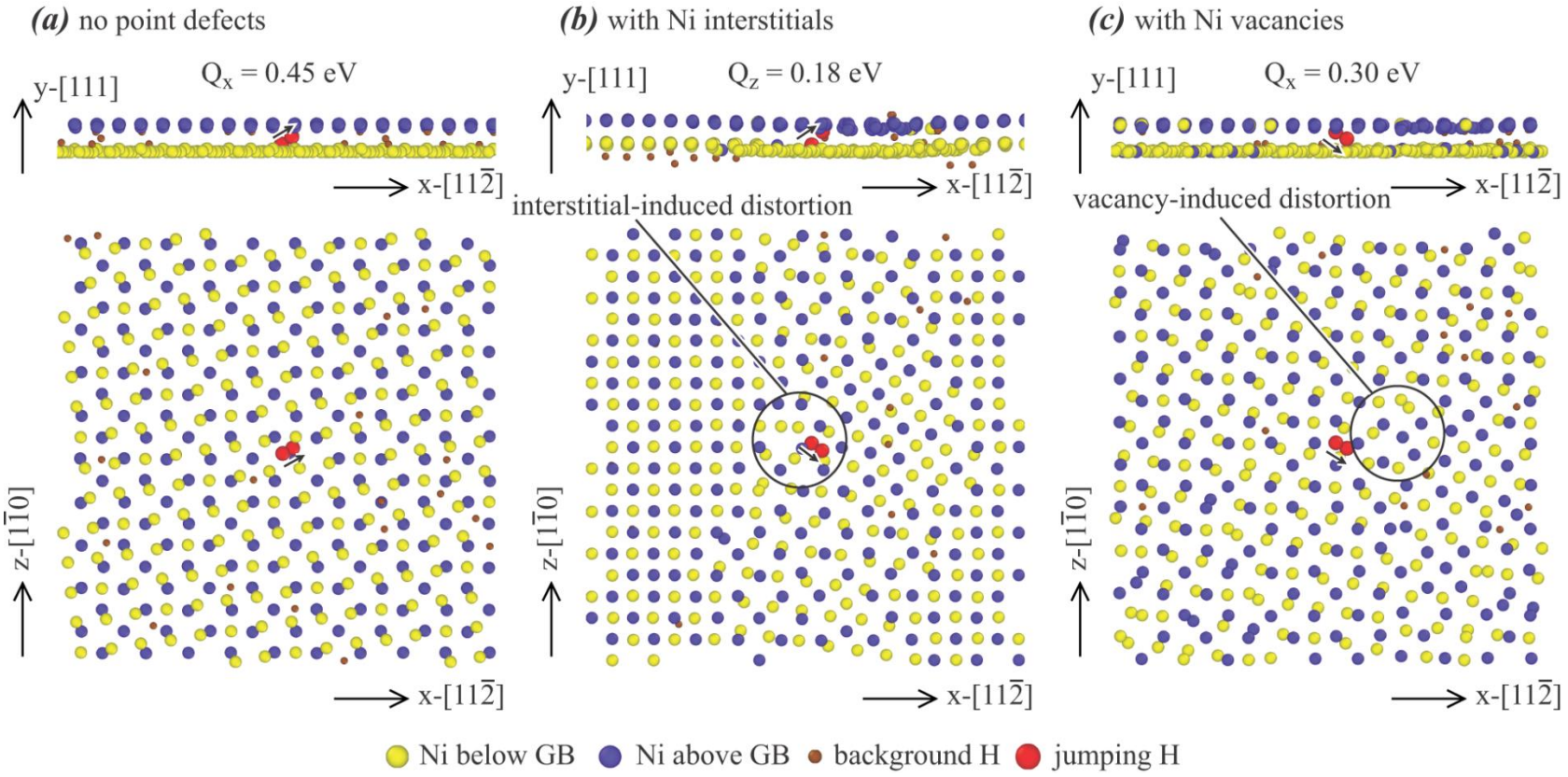

- Presence of nickel interstitials or vacancies can reduce the energy barrier of some hydrogen jump paths further from GB effects alone
- Both interstitials and vacancies cause local distortion

Visualization of Atomic Jumps near the Σ11 GB

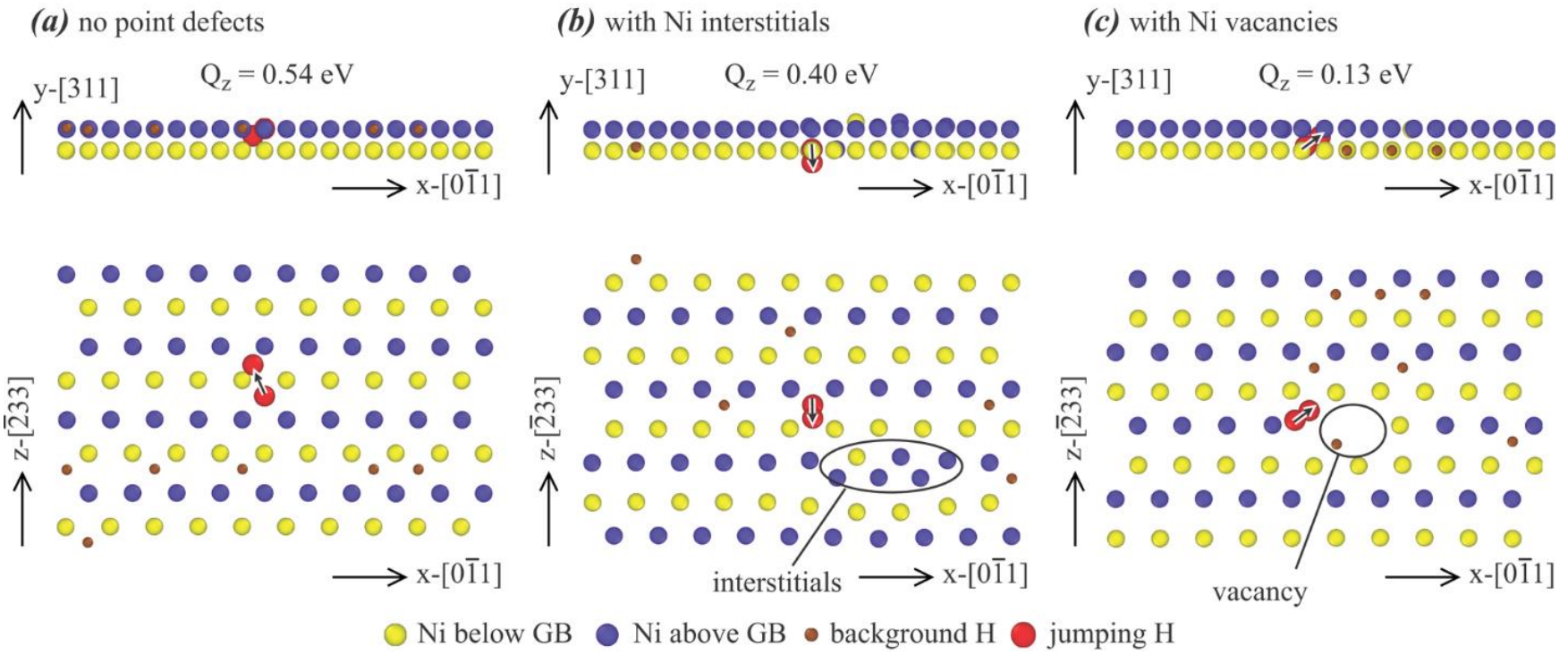

- Presence of nickel interstitials or vacancies can reduce the energy barrier of some hydrogen jump paths further from GB effects alone
- Local interstitials and vacancies are more clearly defined than the Σ5 grain boundary case

Major Conclusions

1. Robust MD diffusion simulation methods have been developed to account for statistical interactions between diffusion species, grain boundaries, and irradiated defects. Highly converged results with almost no statistical errors are demonstrated
2. The predicted activation energy of H diffusion in defect-free single crystal Ni, 0.51 eV, compares well with the experimental value, 0.40 eV
3. For single crystals, 0.5% interstitial increases H diffusivities by 16.3 times at 300 K and 1.4 times at 600 K as compared with perfect crystals. Vacancy does not sensitively change diffusivities
4. Interstitials cause different reconstructions of $\Sigma 3\{111\}$ grain boundaries. Some reconstructions may have significantly increased on-plane H diffusivities: by 146.7 times at 300 K and 2.4 times at 600 K as compared with the boundary alone case
5. Defects significantly increase on-plane H diffusivities on $\Sigma 5\{100\}$ grain boundary
6. $\Sigma 5\{100\}$ and $\Sigma 11\{311\}$ grain boundaries have significant H trapping effects, leading to significantly reduced out-plane H diffusivities
7. Molecular statics calculations of energy barriers of individual jumps help understand the mechanisms of diffusivity changes

The Development of Fe-Ni-Cr Potential

- The real material applied is stainless steels, not nickel
- Bonny et al also have an earlier version of the Fe-Ni-Cr potential (MSMSE, 19, 085008, 2011). Tong et al also developed a MEAM Fe-Ni-Cr-N potential recently (Molecular Simulation, 42, 1256, 2016). We are currently evaluating both potentials
- We are also developing an Fe-Ni-Cr EAM potential suitable for our applications where stacking fault energy and lattice constant are important
- In addition to the conventional fitting of selected properties, we require our potential to capture a single austenitic phase at high temperatures, and coexistence of ferritic and austenitic phases at low temperatures
- Validate the stability of our potential using vapor deposition simulations
- All the results are obtained from time-averaged MD simulations

Issues of EAM Formulation

$$E = \sum_{i=1}^{N} F_I(\rho_i) + \frac{1}{2}\sum_{\substack{i=1 \\ j\neq i}}^{N}\sum^{N} \phi_{IJ}(r_{ij})$$

Embedding energy — Pair energy

$$\rho_i = \sum_{\substack{j=1 \\ j\neq i}}^{N} \rho_J^a(r_{ij})$$

Electron density

- For elemental systems, any linear term added to the embedding energy can be exactly subtracted by a linear term in the pair energy

$$\sum_{i=1}^{N}\left[F_I(\rho_i) + k\rho_i\right] + \frac{1}{2}\sum_{\substack{i=1 \\ j\neq i}}^{N}\sum^{N}\left[\phi_{IJ}(r_{ij}) - 2k\rho_J^a(r_{ij})\right] = \sum_{i=1}^{N} F_I(\rho_i) + \frac{1}{2}\sum_{\substack{i=1 \\ j\neq i}}^{N}\sum^{N}\phi_{IJ}(r_{ij})$$

- Any factor multiplied to the electron density can be exactly divided away in the embedding energy. This impacts alloys

$$F_I(\rho_i) = F_I\left[k \cdot \left(\frac{\rho_i}{k}\right)\right]$$

- These result in poor parameterization

Sandia National Laboratories

Pacific Northwest NATIONAL LABORATORY

Improved Embedding Energy Function

- Requiring zero derivatives independently for embedding and pair energies for the equilibrium phase removes one flexibility. Using relative electron density ρ/ρ_e removes the other flexibility that helps the alloy parameterization
- Our splined embedding energy function has three advantages: removes both flexibilities, has the correct shape, and can be fitted to up to the third derivative

$$F_I(\rho)=\begin{cases}\sum_{i=0}^{3} f_{ni,I}\left(\frac{\rho}{\rho_{n,I}}-1\right)^i, & \rho<\rho_{n,I},\rho_{n,I}=s_{1,I}\rho_{e,I}\\ \sum_{i=0}^{3} f_{i,I}\left(\frac{\rho}{\rho_{e,I}}-1\right)^i, & \rho_{n,I}\le\rho<\rho_{m,I},\rho_{m,I}=s_{2,I}\rho_{e,I}\\ f_{e0,I}+f_{e1,I}\left(\frac{\rho}{\rho_{m,I}}-1\right)+\frac{2f_{e2,I}}{\eta_I}\left[\sqrt{1+\eta_I\left(\frac{\rho}{\rho_{m,I}}-1\right)^2}-1\right], & \rho_{m,I}\le\rho\end{cases}$$

Sandia National Laboratories

Pacific Northwest NATIONAL LABORATORY

Improved Cutoff

- A cutoff function is proposed to take the form of

$$f_{c,IJ}(r) = \begin{cases} \frac{1}{2}\,\mathrm{erfc}\left[\frac{\mu(r - r_{s,IJ}) + \nu(r_{c,IJ} - r)}{r_{c,IJ} - r_{s,IJ}}\right], & r < r_{c,IJ} \\ 0, & r \geq r_{c,IJ} \end{cases}$$

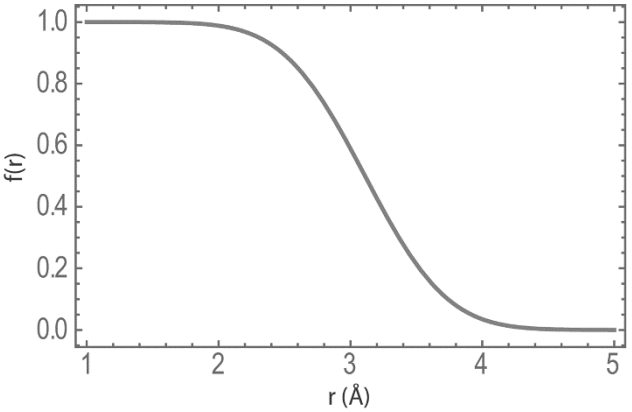

where $\mathrm{erfc}(\mu) = 10^{-5}$, $\mathrm{erfc}(\nu) = 0.9$

- Multiply this cutoff function to any pair function will not change the value of the pair function, but will allow the pair function to be cutoff with continuous high order derivatives
- More importantly, this cutoff function will allow the cutoff distance to be treated as a fitting parameter

Properties of Selected Elemental Phases

Calculated (cal.) and target (tar.) values of lattice constants a and c (Å), cohesive energy E_c (eV/atom), and elastic constants C_{11}, C_{12}, and C_{44} (eV/Å^3) for various elemental structures. ----: non-existing, /: uncalculated or not available, *: experimental [1-4], †: our DFT calculations.

material structure		a		c		E_c		C_{11}		C_{12}		C_{44}	
		cal.	tar.	cal.	tar.	cal.	tar.	cal.	tar.	cal.	tar.	cal.	tar.
Fe	*fcc*	3.63	3.47†	----	----	-4.280	-4.866†	1.27	2.02†	0.79	0.66†	0.84	1.25†
	bcc	2.87	2.87*	----	----	-4.280	-4.280*	2.10	1.52*	1.06	0.86*	1.05	0.76*
	hcp	2.57	2.43†	4.09	3.97†	-4.278	/	/	/	/	/	/	/
Ni	*fcc*	3.52	3.52*	----	----	-4.432	-4.432*	1.63	1.63*	0.94	0.94*	0.82	0.82*
	bcc	2.75	2.80†	----	----	-4.305	-4.697†	0.14	0.93†	0.50	1.32†	0.34	1.02†
	hcp	2.48	2.49†	4.18	4.06†	-4.392	/	/	/	/	/	/	/
Cr	*fcc*	3.66	3.62†	----	----	-4.090	-3.734†	1.44	0.12†	1.00	2.19†	0.73	-0.57†
	bcc	2.88	2.88*	----	----	-4.094	-4.094*	2.67	2.46*	1.14	0.95*	0.83	0.55*
	hcp	2.59	2.56†	4.12	4.18†	-4.084	/	/	/	/	/	/	/

[1] J. D. H. Donnay, and H. M. Ondik, Crystal Data, Determinative Tables, 3rd ed., Vol. 2 (inorganic compounds) (U. S. Department of Commerce, National Bureau of Standards, and Joint Committee on Power Diffraction Standards, U. S. A., 1973)

[2] I. Barin, Thermochemical Data of Pure Substances (VCH, Weinheim, 1993)

[3] G. Simmons, and H. Wang, Single Crystal Elastic Constants and Calculated Aggregate Properties: A Handbook (MIT Press, Cambridge, 1971)

[4] Palmer, S. B.; Lee, E. W. The elastic constants of chromium. Philos. Mag. 1971, 24, 311

Relative Change of Energy and Volume of Alloys with respect to Elements

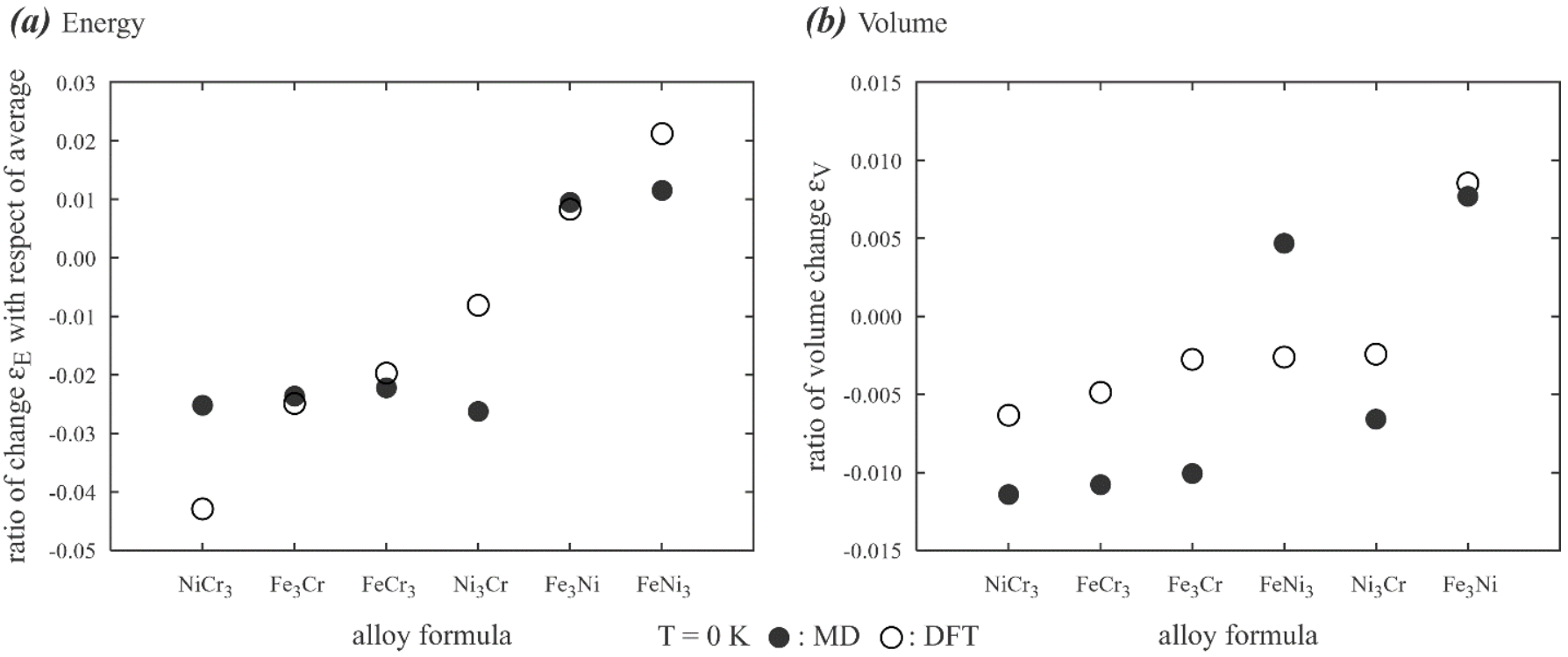

General trends match well between MD and DFT calculations

Sandia National Laboratories

Pacific Northwest NATIONAL LABORATORY

Elastic Constants

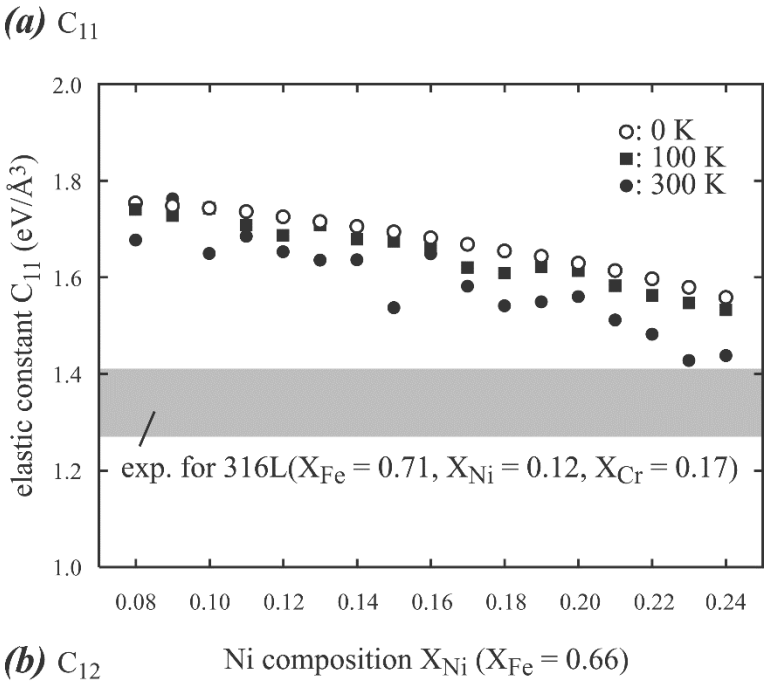

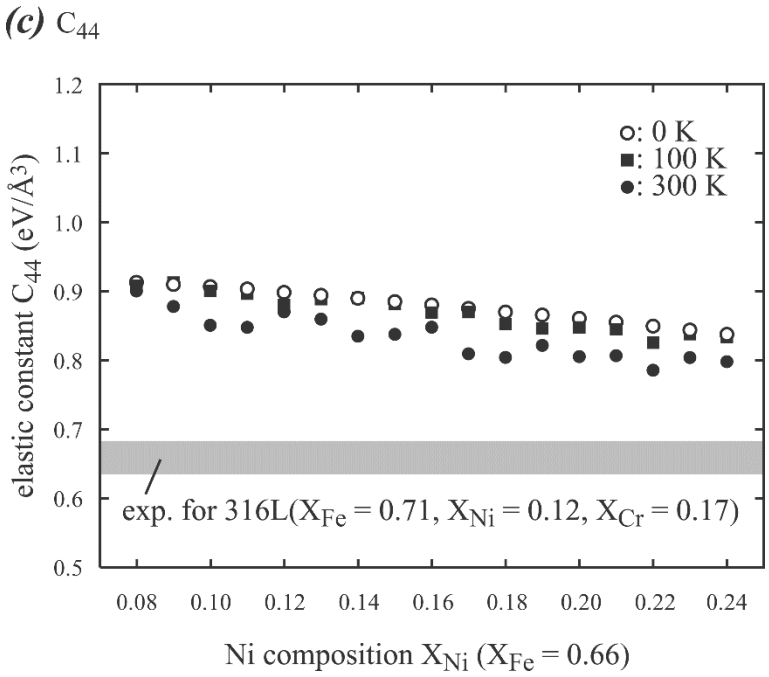

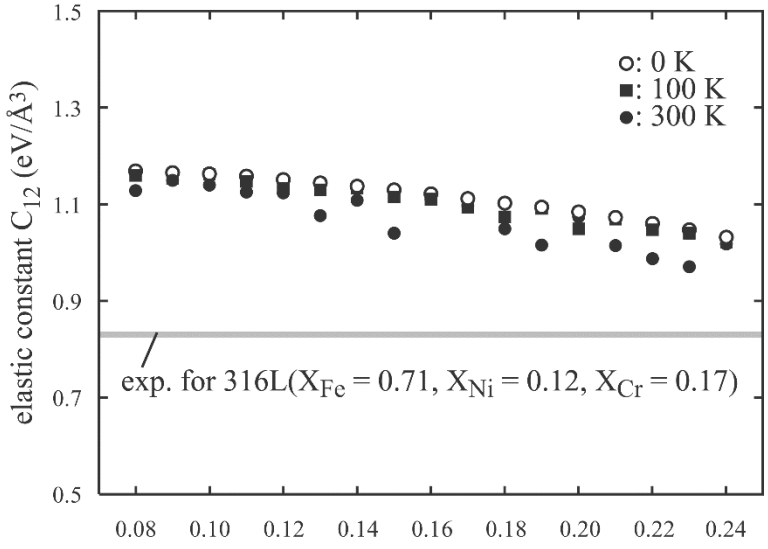

The elastic constants prescribed by the potential for alloys with X_{Fe} = 0.66 seems to be slightly higher than the experimental values for 316L with X_{Fe} = 0.70, taken from Bonny et al, MSMSE, 19, 085008, 2011.

Sandia National Laboratories

Pacific Northwest NATIONAL LABORATORY

Stacking Fault Energy

Molecular Dynamics Results

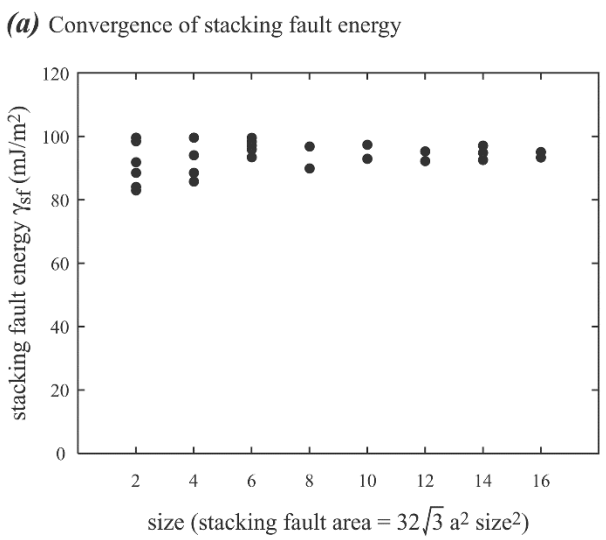

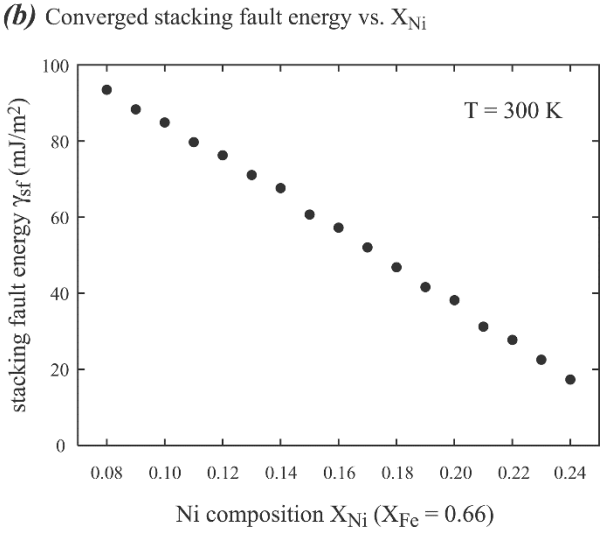

Experimental data from Schramm and Reed, Metall. Trans. A, 6, 1345 (1975).

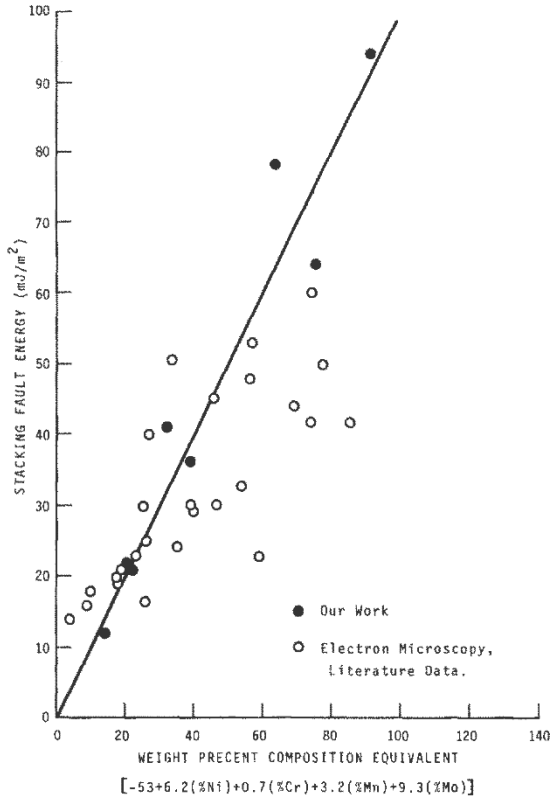

Fig. 4--Relationship between stacking fault energy and Fe-Ni-Cr-Mn-Mo composition in austenitic stainless steels.

The calculated stacking fault energy seems to be in the right order of magnitude

Sandia National Laboratories

Pacific Northwest NATIONAL LABORATORY

Gibbs Free Energy of Mixing ΔG

Time-Averaged MD Calculations of ΔG and ΔH

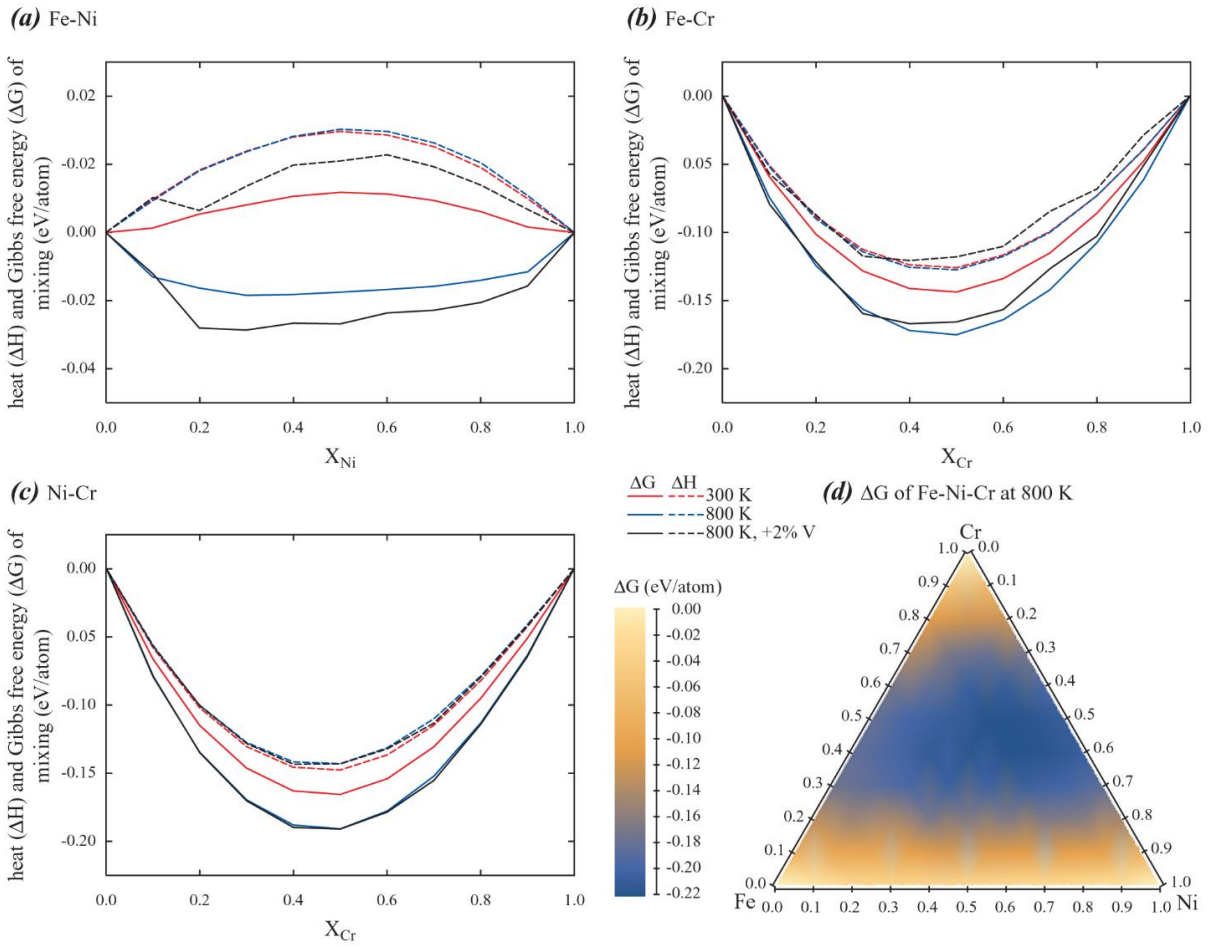

Our potential predicts single austenitic phase at high temperatures, sufficient for model 316L and 304L stainless steels

ASM Phase Diagram © 2016

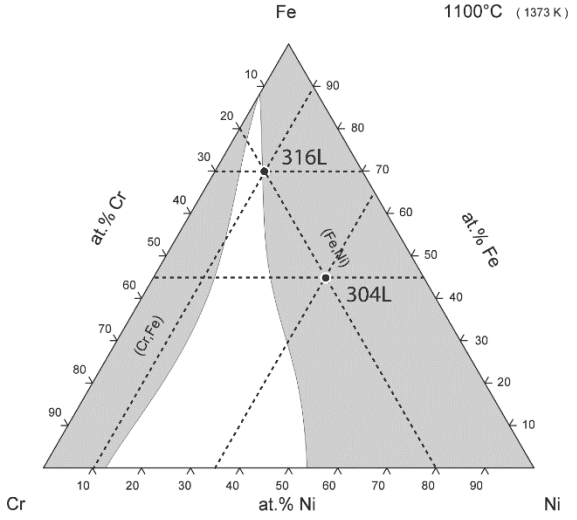

Sandia National Laboratories

Pacific Northwest NATIONAL LABORATORY

Growth Simulation Validation

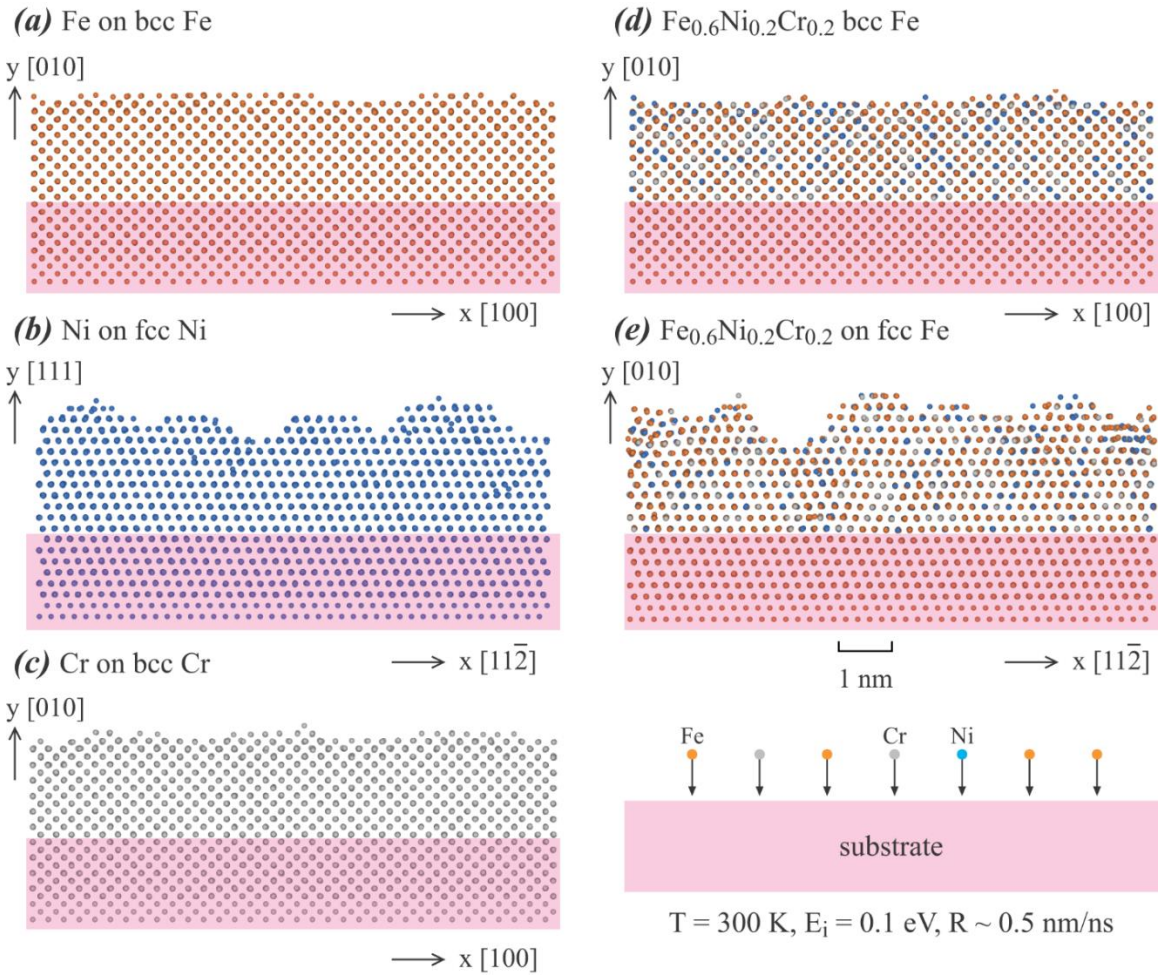

Crystalline growth is achieved for all observed phases, validating their stability in MD simulations

Sandia National Laboratories

Pacific Northwest NATIONAL LABORATORY

Major Conclusions

- Our new Fe-Ni-Cr EAM potential may be appropriate for studying mechanical properties of stainless steels
- The most significant advantages of the potential is that it enables stable simulations of the austenitic phase as well as co-existence of ferritic and austenitic phases

Sandia National Laboratories

Pacific Northwest NATIONAL LABORATORY

Uncertainty Quantification: Ultimate Goal of Models

- Accuracy of interatomic potentials (likely not impact mechanisms and trends)
- Accuracy of molecular dynamics (MD) itself
  - ❑ Models that are absolutely accurate (e.g., dislocation core energy, diffusion energy barriers)
  - ❑ Models that we strongly believable (e.g., thin film structures)
  - ❑ Models that are plausible (e.g., dislocation mediated charge transport in TlBr)

MD Uncertainty Quantification Methods

- MD can inform engineering scale models because when MD results are used as inputs, these models should make exactly the same predictions as MD regardless the potential
- All MD simulations involve statistical errors, but these errors can be quantified and reduced

The total MD simulated time t_{tot} is divided into N segments $t_i = i\Delta t$ ($i = 1, 2, \ldots, N$, $\Delta t = t_{tot}/N$). Each MD simulation produces N values of the time-averaged property P_i for each of the time intervals $\Delta t_i = t_i - t_{i-1} = \Delta t$. As a result, the best estimate of the property can be calculated as

$$\overline{P} = \frac{\sum_{i=1}^{N} P_i}{N} \quad (1)$$

The uncertainty of the samples P_i can be quantified by the sample standard deviation defined as

$$\sigma = \sqrt{\frac{\sum_{i=1}^{N} (P_i - \overline{P})^2}{N-1}} \quad (2)$$

The best estimate $\overline{P}$ is also associated with an uncertainty $\overline{\sigma}$

$$\overline{\sigma} = \frac{\sigma}{\sqrt{N}} \quad (3)$$

Absolutely Accurate Example I: Dislocation Core Energy Calculation

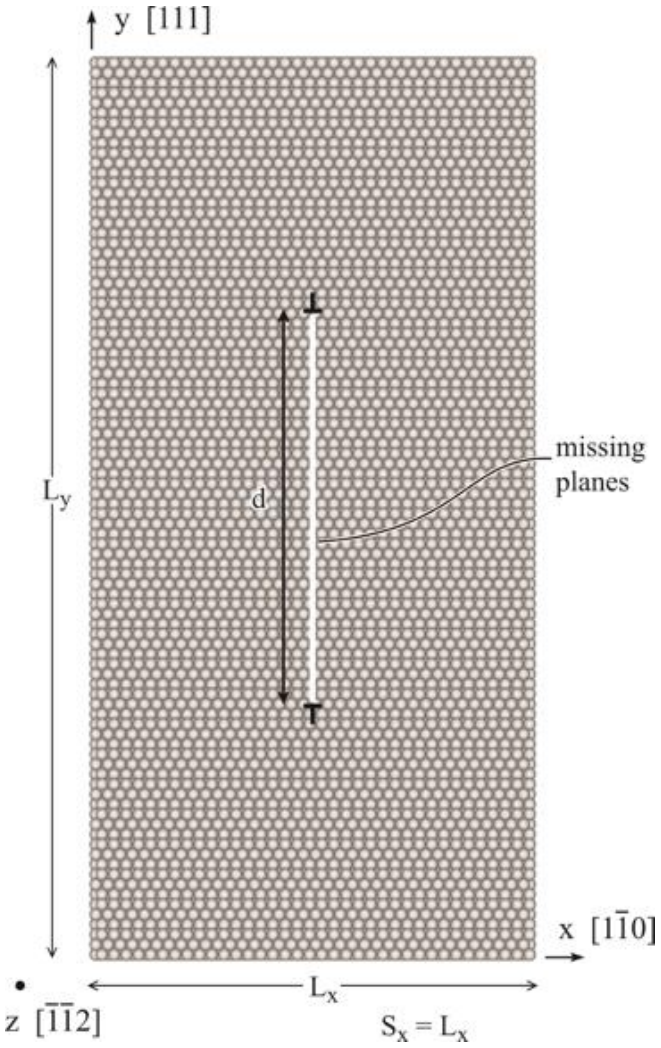

- One can always create a perfect crystal and a crystal containing dislocations under the periodic boundary condition
- Energy of the perfect crystal can always be scaled towards the same number of atoms of the dislocated crystal
- Dislocation energy can always be calculated as the (scaled) energy difference between the dislocated and perfect crystals, without any assumptions
- Dislocation core energy can always be fitted to the continuum solution of the total dislocation energy

Continuum Energy Expression

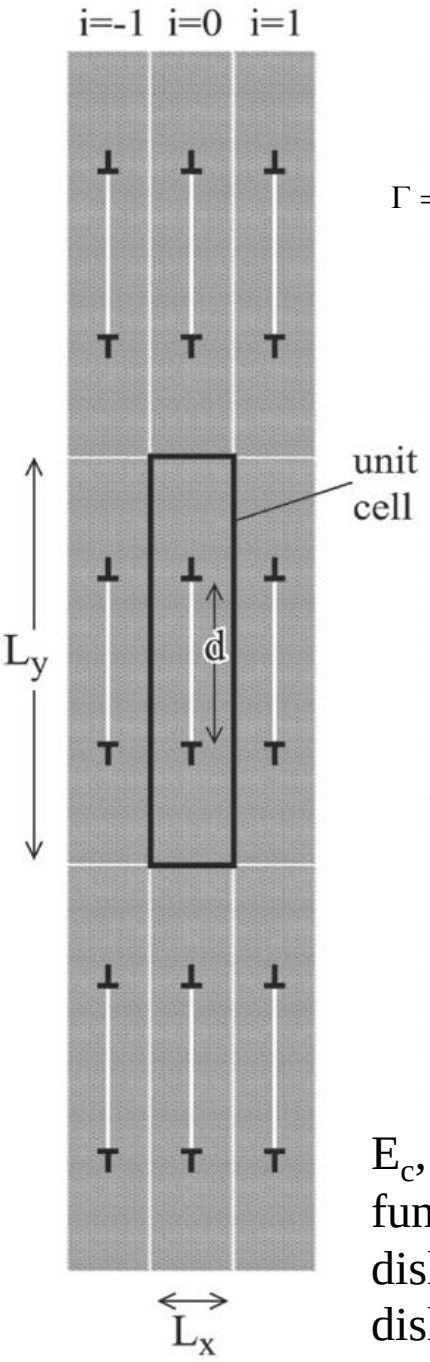

$$\Gamma = E_c + \frac{Gb^2}{4\pi(1-\nu)} \cdot \cos^2\alpha + \sin^2\beta \cdot E_{0,edge} + \cos^2\beta \cdot E_{0,screw} + 2\sin^2\beta \cdot \sum_{i=1}^{\infty} E_{i,edge} + 2\cos^2\beta \cdot \sum_{i=1}^{\infty} E_{i,screw}$$

$$E_{0,edge} = \frac{Gb^2}{4\pi(1-\nu)} \left\{ \ln\left(\frac{d}{r_0}\right) + \ln\left(\frac{L_y - d}{L_y}\right) - \ln\left[Ga\left(\frac{L_y + d}{L_y}\right)\right] - \ln\left[Ga\left(2 - \frac{d}{L_y}\right)\right] \right\}$$

$$E_{0,screw} = \frac{Gb^2}{4\pi} \left\{ \ln\left(\frac{d}{r_0}\right) + \ln\left(\frac{L_y - d}{L_y}\right) - \ln\left[Ga\left(\frac{L_y + d}{L_y}\right)\right] - \ln\left[Ga\left(2 - \frac{d}{L_y}\right)\right] \right\}$$

$$E_{i,edge} = \frac{Gb^2}{8\pi(1-\nu)} \left\{ \frac{4\pi \cdot i \cdot L_x \cdot \coth\left(\frac{\pi \cdot i \cdot L_x}{L_y}\right) \cdot \sin^2\left(\frac{\pi \cdot d}{L_y}\right)}{L_y \cdot \cosh\left(\frac{2\pi \cdot i \cdot L_x}{L_y}\right) - L_y \cdot \cos\left(\frac{2\pi \cdot d}{L_y}\right)} + \ln\left[\cos^2\left(\frac{\pi \cdot d}{L_y}\right) + \coth^2\left(\frac{\pi \cdot i \cdot L_x}{L_y}\right) \cdot \sin^2\left(\frac{\pi \cdot d}{L_y}\right)\right] \right\}$$

$$E_{i,screw} = \frac{Gb^2}{8\pi} \ln\left[\cos^2\left(\frac{\pi \cdot d}{L_y}\right) + \coth^2\left(\frac{\pi \cdot i \cdot L_x}{L_y}\right) \cdot \sin^2\left(\frac{\pi \cdot d}{L_y}\right)\right]$$

E_c independent of geometry!

E_c, r_0: core energy, radius, Ga: Euler gamma function, coth, cosh: hyperbolic functions, G, ν: shear modulus, Poisson's ratio, b: Burgers magnitude, α: dislocation dipole direction (α = 0° means vertical dislocation dipole), β: dislocation character angle

Time Averaged MD Simulations ⇒ Convergence

Edge Dislocation

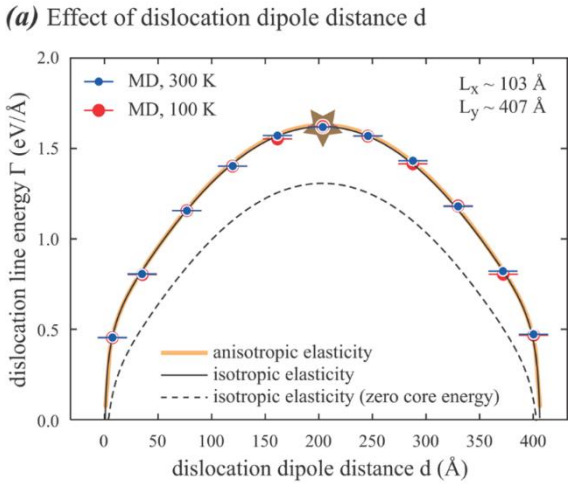

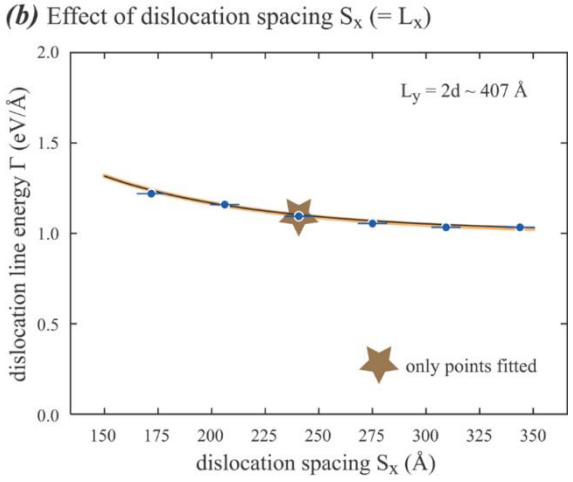

Mixed Dislocations

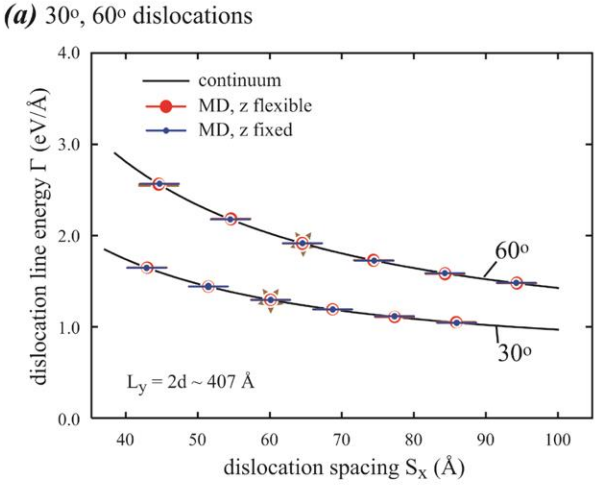

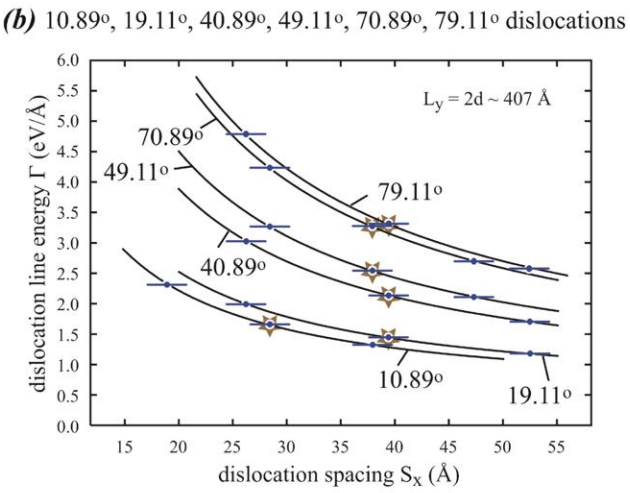

Screw Dislocation

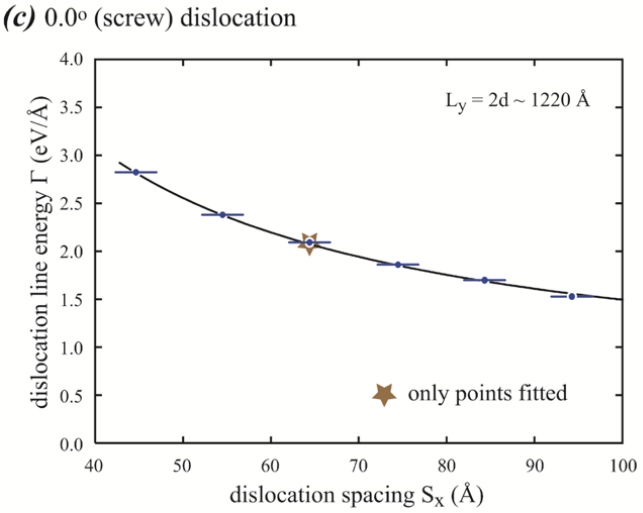

- Negligible error bars
- No time scale issue because error bars are already negligible
- No length scale issues because already captures the continuum solutions

Absolutely Accurate MD Can Validate and Correct Classical Theories

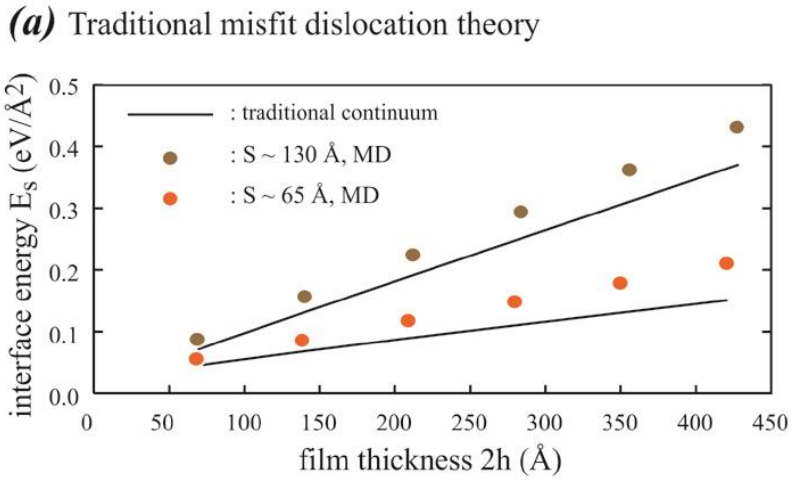

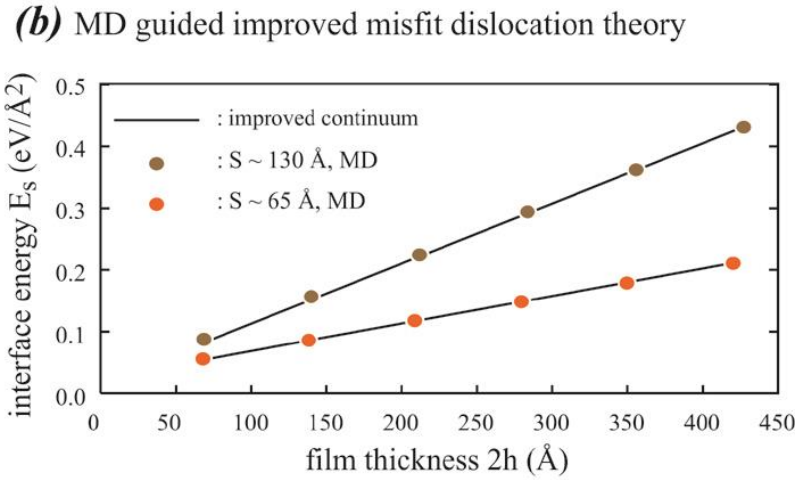

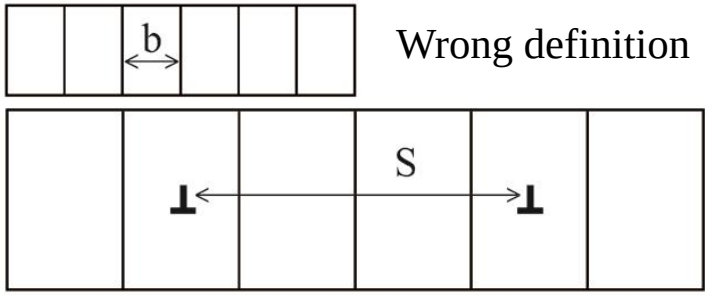

Wrong definition

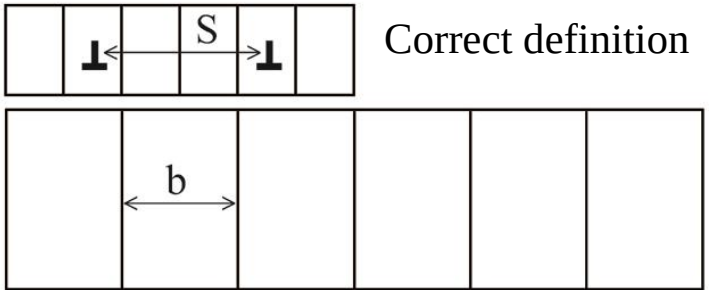

Correct definition

- **Continuum misfit dislocation theory has been widely used since 1980's**
- **MD simulations revealed that traditional continuum misfit dislocation theory is incorrect in the definition of dislocation Burgers vector and dislocation spacing**
- **This example indicates that absolutely accurate MD can "validate" and improve continuum models**

Absolutely Accurate Example II: Diffusion Energy Barrier Calculation

- Without assuming atomic jump paths, the coordinates $\alpha_i(t)$ of diffusing atoms (i = 1, 2, …, N), are recorded every Δt, i.e., at times of $t = j\Delta t$, j = 1, 2, …, m ($m = t_{MD}/\Delta t$), where Δt can be any multiple of the time step size dt used in the MD simulations
- m+1-k measurements can be made for the displacement of each diffusing atom i over a $k\Delta t$ period: $\Delta\alpha_{i,j}(k\Delta t) = \alpha_i(j\Delta t - \Delta t + k\Delta t) - \alpha_i(j\Delta t - \Delta t)$ where j = 1, 2, …, m+1-k.
- This allows us to calculate mean square displacement (MSD):

$$\left\langle \left[\Delta\alpha(k\Delta t)\right]^2 \right\rangle = \frac{\sum_{i=1}^{N}\sum_{j=1}^{m+1-k}\left[\Delta\alpha_{i,j}(k\Delta t)\right]^2}{N(m+1-k)}$$

- MSD can be fitted to diffusivities D:

$$\left\langle \left[\Delta\alpha(k\Delta t)\right]^2 \right\rangle = 2D_\alpha t$$
$$\left\langle \left[\Delta x(k\Delta t)\right]^2 \right\rangle + \left\langle \left[\Delta z(k\Delta t)\right]^2 \right\rangle = 4D_{xz} t$$
$$\left\langle \left[\Delta x(k\Delta t)\right]^2 \right\rangle + \left\langle \left[\Delta y(k\Delta t)\right]^2 \right\rangle + \left\langle \left[\Delta z(k\Delta t)\right]^2 \right\rangle = 6D_{xyz} t$$

MSD Convergence Example

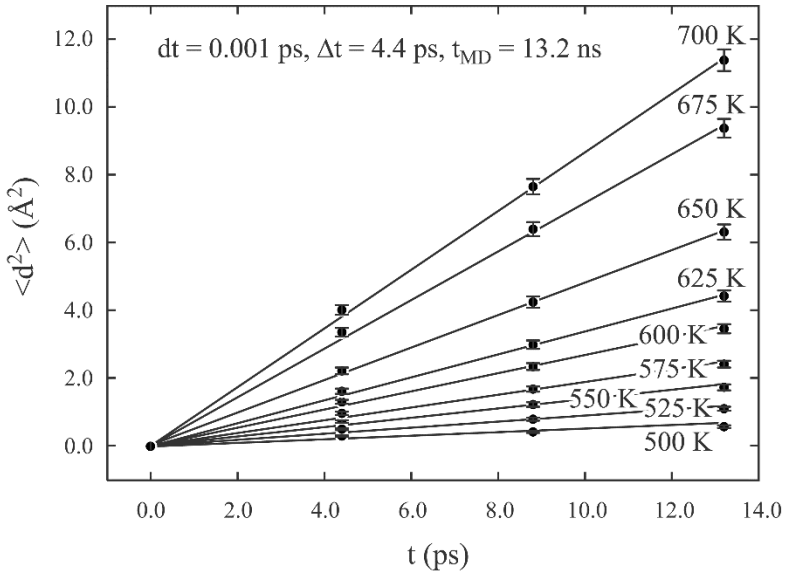

Zhou et al, J. Phys. Chem. C, 120, 7500 (2016).

Time Averaged MD Simulations ⇒ Convergence

Diffusion of Hydrogen in PdH_x

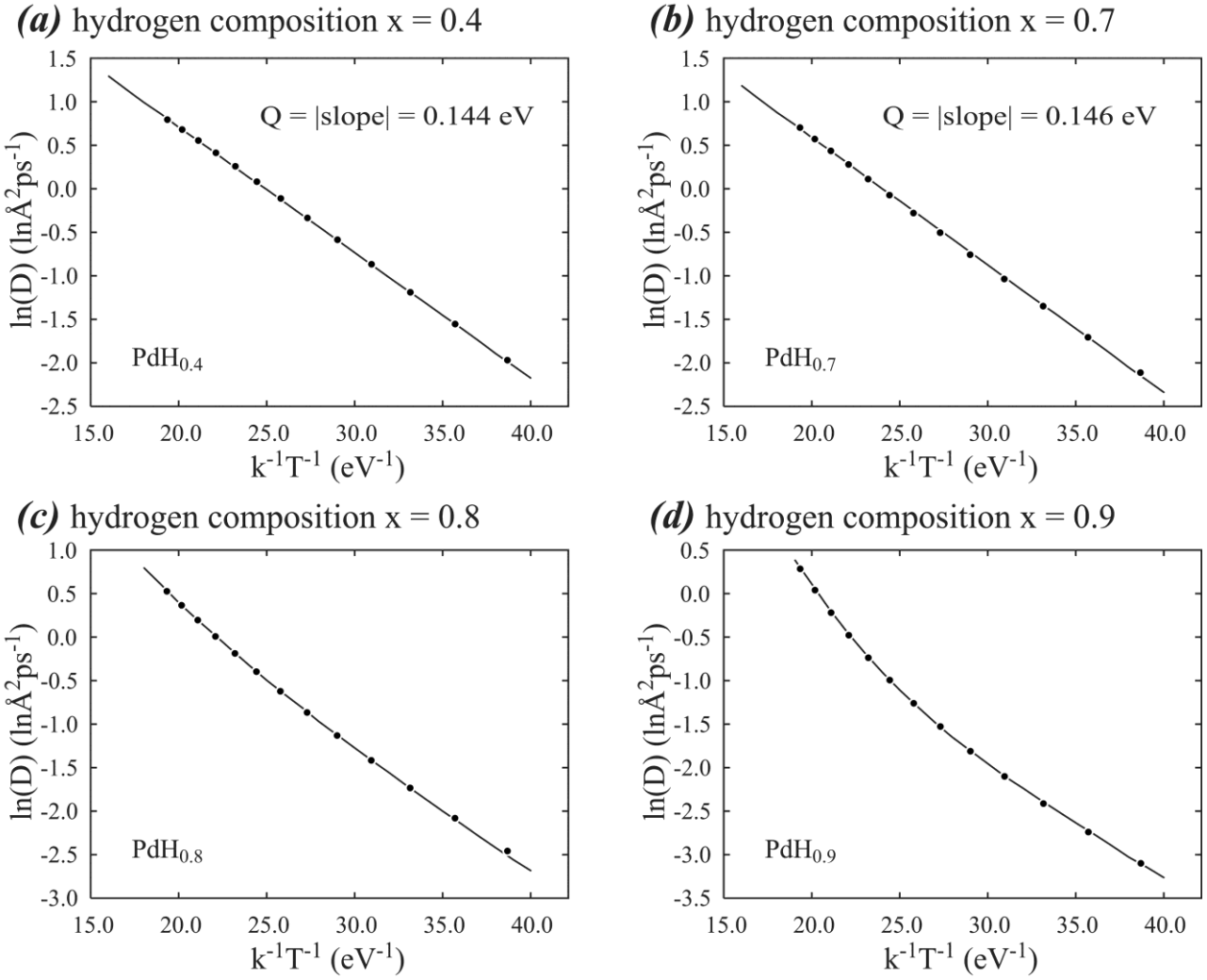

- Negligible error bars
- No time scale issue because error bars are already negligible
- No length scale issues because the computational cell can include all geometries of our problems (e.g., grain boundaries)

Major Conclusions

Time-averaged molecular dynamics simulations can be used to calculate accurate dislocation core energy and diffusion energy barriers. While the interatomic potential used in the simulations has errors, the simulations do not introduce additional non-negligible errors regardless time and length scales